Materials Today Bio 25 (2024) 100982

Contents lists available at ScienceDirect

Materials Today Bio

journal homepage: www.journals.elsevier.com/materials-today-bio

Near-infrared light responsive gold nanoparticles coating endows polyetheretherketone with enhanced osseointegration and antibacterial properties

Xinxin Zhan [a], Jianglong Yan [b], Dong Xiang [a], Hao Tang [a], Lulu Cao [a], Yufeng Zheng [c], Hong Lin [a,**], Dandan Xia [a,*]

[a] Department of Dental Materials, National Center of Stomatology, National Clinical Research Center for Oral Diseases, National Engineering Research Center of Oral Biomaterials and Digital Medical Devices, Beijing Key Laboratory of Digital Stomatology, Research Center of Engineering and Technology for Computerized Dentistry Ministry of Health, NMPA Key Laboratory for Dental Materials, Beijing, 100081, China
[b] Simpson Querrey Institute for BioNanotechnology, Northwestern University, Chicago, IL, 60611, USA
[c] School of Materials Science and Engineering, Peking University, Beijing, 100871, China

ARTICLE INFO

Keywords:
Polyetheretherketone
Gold nanoparticles
Metronidazole
Near-infrared
Antibacterial
Osseointegration

ABSTRACT

Polyetheretherketone (PEEK) is considered as a promising dental implant material owing to its excellent physicochemical and mechanical properties. However, its wide range of applications is limited by its biologically inert nature. In this study, a near-infrared (NIR) light responsive bioactive coating with gold nanoparticles (AuNPs) and metronidazole adhered to the PEEK surface via dopamine polymerization. Compared to pure PEEK, the hydrophilicity of the treated PEEK surface was significantly improved. In addition, under NIR light, the surface coating exhibited photothermal conversion effect, and gold nanoparticles and the antibiotic can be released from the coating. This improved the antibacterial properties of PEEK materials. Moreover, the coating was more conducive to the early adhesion of bone mesenchymal stem cells. The results of *in vitro* and *in vivo* osteogenic activity studies showed that the developed coating promoted osseointegration of PEEK implants, and NIR light irradiation further improved the antibacterial ability and osteogenic activity of PEEK implants. Through RNA sequencing, the potential underlying mechanism of promoting bone formation of the AuNPs coating combined metronidazole was interpreted. In summary, the developed coating is a potential surface treatment strategy that endows PEEK with enhanced osseointegration and antibacterial properties.

1. Introduction

In the field of dental implants, the stress-shielding effect of implant materials such as pure titanium and titanium alloys, might leading to marginal bone loss [1]. And metal materials may cause metal ion allergy or anterior teeth unaesthetic [2]. Thus, many researchers are dedicated to explore more suitable materials for dental implant restoration. In view of the advantages of polyetheretherketone (PEEK) material, including good cell compatibility, stable chemical structure, not easy to degrade, no free radicals and other toxic substances' precipitation, and radiolucency, it has been proposed as a promising dental implant material [3]. However, it is biologically inert. After PEEK materials implanted into bone tissue, fibrous encapsulation was formed firstly on its surface [4,5]. Furthermore, some studies have pointed out that the antibacterial ability of the PEEK materials is poor [6,7]. Therefore, it is necessary to develop modification methods to improve the antibacterial and osteogenic ability of PEEK materials.

Currently, antibiotics therapy remains the primary approach for treating infection, which can be administered systemically or locally. In these treatment strategies, antibiotics can also be combined onto the surface of implants to provide the implants antibacterial capability for resisting bacterial infections [7]. In previous studies, the antibacterial

* Corresponding author. Department of Dental Materials, Peking University School and Hospital of Stomatology, No.22, Zhongguancun South Avenue, Haidian District, Beijing, 100081, China.
** Corresponding author. Department of Dental Materials, Peking University School and Hospital of Stomatology, No.22, Zhongguancun South Avenue, Haidian District, Beijing, 100081, China.
E-mail addresses: hong196lin@bjmu.edu.cn (H. Lin), dandanxia@pku.edu.cn (D. Xia).

https://doi.org/10.1016/j.mtbio.2024.100982
Received 12 November 2023; Received in revised form 16 January 2024; Accepted 25 January 2024
Available online 1 February 2024

effects of antibiotics coatings were mainly investigated against *Staphylococcus aureus* and *Escherichia coli*. Regarding the peri-implantitis, the research demonstrated that the dominant pathogenic bacteria is *Porphyromonas gingivalis* (*P. gingivalis*) [8,9], a gram-negative anaerobic bacterium. It's well known that metronidazole (M) is a commonly used antibiotic for the treatment of systematic or local infections caused by anaerobic bacteria [10], such as periodontitis [11,12]. In addition, metronidazole was also used in the occlusive periodontal membrane to assist in periodontal tissue regeneration [13,14].

Although the antibiotic coating on the surface of implants can provide excellent antibacterial properties, the emergence of drug-resistant bacteria is also a challenge that needs to be addressed [15]. Nowadays, metal nanoparticles coating, such as Ag^{+}, were developed to enhance the antibacterial performance of PEEK material [7]. But at the same time, the toxicity of high concentrations of metal ions to normal cells [16], and the emergence of silver-resistant bacteria [17] have attracted widespread attention. Research findings suggested that gold nanoparticles (AuNPs) have highly biological safety [18,19] and antibacterial properties [20]. And it rarely developed antibacterial resistance at present [21,22]. Moreover, the combination of AuNPs and antibiotics could exhibit better antibacterial effect, which could reduce the use of antibiotics and produce a synergistic antibacterial effect [22,23].

The improvement in the antibacterial capability of implants can alleviate inflammation after implantation, while the enhancement of osteogenic activity is essential to ensure long-term stability of the PEEK implants. Research showed that AuNPs can stimulate an inflammatory response, and the anti-inflammatory effects of AuNPs promoted the osteogenic differentiation of BMSCs *in vitro* [20]. What's more, in view of the good optical properties of AuNPs, they can be used as photosensitizers for near-infrared (NIR) light to undergo photothermal conversion [24]. The NIR light can increase the local temperature with help of AuNPs [25]. And the mild heat shock conditions (39–41°C) can successfully upregulate the expression of proteins such as alkaline phosphatase (ALP) and heat shock protein (HSP), thereby promoting bone mineralization [26].

Herein, we designed a NIR-responsive surface coated with gold nanoparticles and metronidazole, as shown in scheme (Scheme 1). The combination of AuNPs and metronidazole endowed the PEEK materials with better antimicrobial ability. When the PEEK surface coating responds to NIR light, the surface temperature of the PEEK materials could reach around 42°C. And the release of AuNPs was increased after NIR light irradiation. The results of *in vivo* experiments demonstrated that the NIR-responsive surface coating exhibited enhanced antibacterial effects, and the osteogenic properties were significantly improved. In addition, the potential osteogenic mechanism of this coating was illustrated. This approach represents a simpler and safer treatment strategy to improve the antibacterial ability and osteogenic activity of PEEK materials for potential dental implant applications.

2. Materials and methods

2.1. Preparation of the treated PEEK materials

Disc-shaped PEEK (Ensinger, Nufringen, Germany) with dimensions Φ15 × 1.5 mm was used for surface characterization and *in vitro* biological assays, while cylindrical implants with dimensions Φ2 × 5 mm were prepared for rat femoral implantation *in vivo*. Prior to use, the samples were polished with abrasive papers and ultrasonically cleaned in anhydrous ethanol and deionized water for 15 min sequentially, and dried at 70°C.

Gold nanoparticles (AuNPs) were obtained by reducing chloroauric acid (C805628, Macklin, Shanghai, China). More specifically, chloroauric acid (5×10^{-4} M) is mixed with Triton X-100 (1×10^{-2} M) in 40 mL deionized water, then reduced using L-ascorbic acid (3×10^{-2} M). The solution was then centrifuged at 10,000 rpm for 20 min, the supernatant removed, and 5 mL of deionized water was added to resuspend the pellet.

The functionalized PEEK surface was prepared by mixing metronidazole (M, B1976, APExBIO, American), AuNPs, and dopamine hydrochloride (D103111, Aladdin, Shanghai, China). Dopamine hydrochloride was added to a Tris-HCl solution (10 mM, pH 8.5, Solarbio, Beijing, China) at a concentration of 2 mg/mL. The AuNPs and metronidazole solution were added to 1.8 mL of dopamine solution to form a 2 mL mixed solution. Pure PEEK samples were soaked in the mixed solution with gentle shaking at 37°C for 18 h. Depending on the reagents added, the experimental groups consisted of PEEK(P), M/P, AuNPs/P, and M-AuNPs/P. The control group was pure PEEK. The PEEK modified with gold nanoparticles was named AuNPs/P, while the PEEK material modified with metronidazole was named M/P. The PEEK material modified with metronidazole and gold nanoparticles was named M-AuNPs/P. The treated samples were washed with deionized water for 5 min to remove unadhered species.

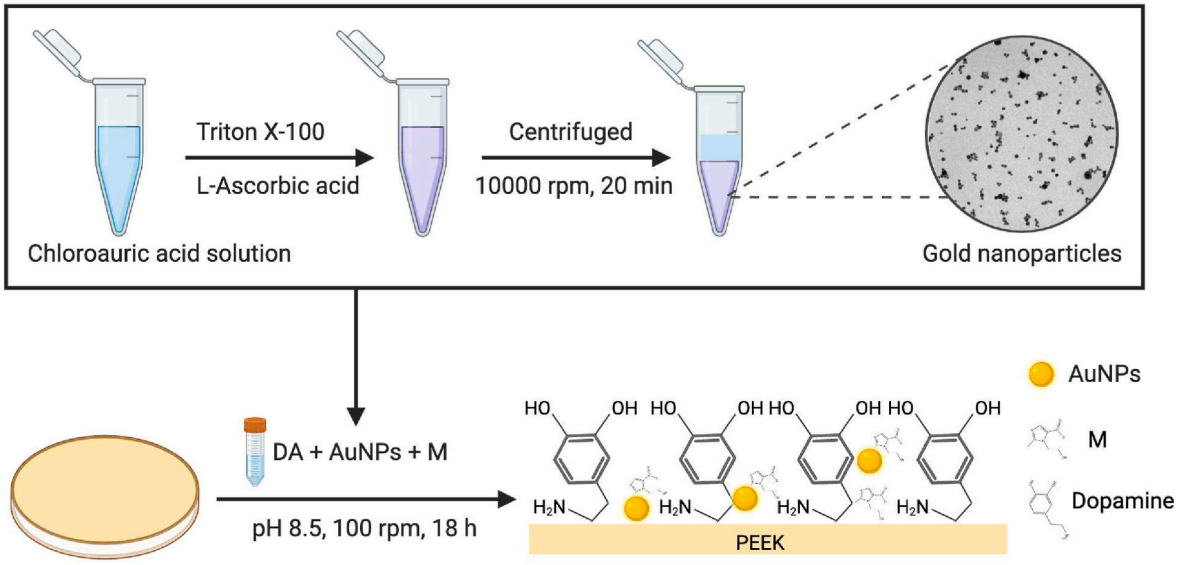

Scheme 1. Schematic illustration of AuNPs preparation and surface functionalization process on PEEK.

2.2. Surface physical and chemical property of PEEK samples

Transmission electron microscopy (TEM, JEM-1400, Leica, Germany) was used to observe the size and degree of gold nanoparticles dispersion. Field-emission scanning electron microscopy (FE-SEM, Hitachi SU8010, Japan) was used to observe the morphological characteristics of the treated PEEK surfaces. The roughness of all the groups was evaluated using three-dimensional morphometry laser microscopy (VK-X200, Keyence, Japan) according to the DIN EN ISO 4287 standard. The water contact angle was detected by contact angle goniometer (DSA100, Kruss, Germany). The chemical elements of the different modified PEEK surface were analyzed using X-ray photoelectron spectrscopy (XPS, AXIS Supra, Kratos Analytical Ltd., England). Inductively coupled plasma-mass spectrometry (ICP-MS, Aglient 7800, USA) was used to detect the AuNPs content on the AuNPs modified PEEK surface. The content of released metronidazole was detected using high performance liquid chromatography (HPLC, Agilent HPLC 1260, Japan).

2.3. NIR irradiation

To study the thermal effects of the modified PEEK surfaces, the experimental specimens were placed in phosphate buffered saline and irradiated with an NIR laser (MDL–III–808 nm, Changchun New Industry Photoelectric Technology Co., Ltd., China) at a power density of 1.25 W/cm^2 for 10 min. The temperature of the solution was measured using an infrared thermal camera (Testo 883, Testo AG, Germany).

2.4. Antibacterial assay in vitro

2.4.1. Bacteria culture

The bacteriostatic effect of the various treatment samples on Gram-negative *P. gingivalis* (ATCC 33277) was evaluated. *P. gingivalis* were cultured in brain heart infusion (BHI, Oxoid, Canada) and agar with 5 μg/mL hemin, 5 mg/mL yeast extract, 1 μg/mL vitamin K1, and 1:20 (v/v) defibrinated sheep blood. All samples of *P. gingivalis* were grown in an anaerobic bag (Thermo Fisher) for the scheduled times at 37°C.

2.4.2. Bacterial viability assay

The Microbial Viability Assay Kit-WST (Dojindo) was used to evaluate the antimicrobial activity of the different PEEK specimens. The medium was collected at the predetermined time. The PEEK samples were removed, gently cleaned, and placed into a new 24-well plate. Thereafter, WST reagent was added to each well at a ratio of 1:20 (v/v) to the medium. Following incubation at 37°C in the dark for 2 h, 100 μL of the supernatant was transferred to a 96-well plate and the OD at 450 nm was measured using a microplate reader. The supernatant of bacterial culture was collected, of which 100 μL was used for culture on brain heart infusion (BHI) solid medium. And the colony forming unit (CFU) bacteria were observed after one week.

2.4.3. Live/dead staining of bacteria on the surface of different PEEK samples

The LIVE/DEAD Bacterial Viability Kit (L7007, Invitrogen, USA) was employed to observe the activity of bacteria on different samples surfaces. After culturing bacteria on different sample surfaces for 1 day, the supernatant was removed and gently washed with PBS. The staining reagent was added into the 24-well plate according to the instructions, and the samples were incubated at room temperature in the dark for 15 min. Observation was done using a fluorescence microscope.

2.5. Biocompatibility evaluation in vitro

2.5.1. Cell culture

Human bone mesenchymal stem cells (HBMSCs, Science Cell Research Laboratories, California, USA) were cultured in 5% CO_2 and 100% humidity in alpha-modified minimum essential medium (Gibco, California, USA) containing 10% fetal bovine serum (Gibco, Australia) and 1% penicillin/streptomycin (Gibco, California, USA). Cells at the 4th to 6th generation were chosen and seeded on different PEEK samples at a density of 2×10^4 cells/mL.

2.5.2. Cell morphology and cytoskeletal observation

After culturing for 4 and 24 h, cells on different PEEK surfaces were fixed with 4% paraformaldehyde for 30 min and dehydrated in gradient ethanol (30, 50, 60, 70, 80, 90, and 100%) for 15 min. After gold spraying, the cells were observed using FE-SEM. In addition, after 4 and 24 h of culture, cells on different PEEK surfaces were fixed with 4% paraformaldehyde for 30 min and permeabilized with Triton X-100 (0.1% v/v) for 5 min. They were then incubated with a diluted phalloidin FITC solution (1:400) (Sigma–Aldrich, USA) for 40 min. Finally, the cytoskeletal were examined using laser scanning confocal microscope (Carl Zeiss, Germany).

2.5.3. Cell proliferation assay

Cell proliferation of the different PEEK samples cultured in 24-well was detected using cell counting kit (CCK-8, Dojindo, Japan) at days 1, 3, 5, and 7. The culture medium was mixed with CCK-8 reagent (10:1 v/v) in the dark for 2 h in a 5% CO_2 incubator at 37°C. The solution (100 μL) in each well was transferred to a 96-well plate, and the optical density (OD) was measured at 450 nm using a plate reader (Biotek, ELX808, USA).

2.5.4. Osteogenic bioactivity evaluation in vitro

The human bone mesenchymal stem cells were cultured in osteogenic induction medium containing dexamethasone (10 nM, Sigma), ascorbic acid (200 μM, Sigma) and β-glycerophosphate (10 mM; Sigma) for 7 and 21 days. After 7 days, the expression of bone-associated genes was analyzed using real-time quantitative reverse transcription polymerase chain reaction (RT-qPCR). Total cellular RNA was extracted from the treated samples using TRIzol reagent (Invitrogen), and the Prime Script RT Reagent Kit (Takara, Tokyo, Japan) was used to synthesize cDNA. RT-qPCR was performed using a 7500 HT Fast Real Time PCR System with SYBR Green (Invitrogen). The primer sequences for the bone-associated genes are listed in Table 1. After culturing the cells on different PEEK samples for 21 days, the samples were fixed with 4% paraformaldehyde for 15 min, washing with deionized water, and stained with alizarin red solution (1% w/v, Sigma, USA) in deionized water. Subsequently, 10% m/v cetyl-pyridinium chloride (Sigma) was added to dissolve the red matrix sediment. The OD of the solution was measured at 490 nm OD using a multimode plate reader (PerkinElmer).

2.5.5. The endocytosis of AuNPs into cells

The hBMSCs were cultured on the surface of AuNPs/P group and M-AuNPs/P groups. Some samples of the two groups were exposed to NIR light irradiation on the first day. After 3 days, the cells were collected and counted. The ICP-MS was used to detect the amount of AuNPs in the cells.

2.6. Antibacterial activity of PEEK samples in vivo

2.6.1. Surgical procedure

The animal procedures were approved by the Animal Ethics Committee of Peking University (approval no. LA2021407). We complied with the ARRIVE (Animal Research: Reporting of *In Vivo* Experiments) 2.0 guidelines. Thirty BALB/c mice aged 7 weeks were randomly and evenly divided into three groups, and stocked in SPF laboratory for one week in to acclimatize. Then all the mice were anesthetized using pentobarbital sodium (50 mg/kg). The different PEEK samples (Φ8 × 1 mm) were then implanted into the subcutaneous pockets on the back of BALB/c mice. *P. gingivalis* (10^8 CFU/mL, 0.1 mL) were injected into the surface of different samples. In summary, animal experiments are

Table 1
Primer of osteo-related genes in RT-PCR.

Gene	Forward primers (5′-3′)	Reverse primers (3′-5′)
ALP	ATGGGATGGGTGTCTCCACA	CCACGAAGGGGAACTTGTC
Collagen-1	AGTGGTTTGGATGGTGCCAA	GCACCATCATTTCCACGAGC
BMP6	CAGCCTGCAGGAAGCATGAG	CAAAGTAAAGAACCGAGATG
CCL5	GAGTATTTCTACACCAGTGGCAAG	TCCCGAACCCATTTCTTCTCT
AKT	CACCCAGTGACAACTCAGGG	GGCCACGATGACTTCCTTCT
GAPDH	AGGTCGGTGTGAACGGATTTG	TGTAGACCATGTAGTTGAGGTCA

grouped into PEEK (P), M-AuNPs/P, M-AuNPs/P (NIR+). The backs of M-AuNPs/P (NIR+) group mice were irradiated with NIR light. No experimental animals died during or after surgery. The mice were euthanized using carbon dioxide method at 3 days and 7 days.

2.6.2. Antibacterial assay

The skin tissue around the implants and the specimens were collected. Part of the skin tissue was shredded and placed in saline, and then concussed by ultrasound. The suspension was then used for bacteria culture. The other part of the tissue was soaked in paraformaldehyde, and was used for tissue sections staining. The topography of the surfaces of different specimens was observed by FE-SEM.

2.7. Osteogenic bioactivity in vivo

2.7.1. Surgical implantation

Twenty-four male Sprague Dawley (SD) rats aged 6 weeks were randomly and evenly divided into three cages, and stocked in SPF laboratory for one week to acclimatize. Then all the rats were anesthetized using pentobarbital sodium (50 mg/kg). The different PEEK samples were then implanted into prepared holes (Φ2 × 5 mm using a dental drill) in the rat femurs. In summary, animal experiments are grouped into PEEK (P), M-AuNPs/P, M-AuNPs/P (NIR+). No experimental animals died during or after surgery. The rats were euthanized using carbon dioxide method at 4 and 8 weeks respectively. All the femurs were harvested and fixed with 4% paraformaldehyde for micro-computed tomography (Micro-CT) and histochemical staining.

2.7.2. Micro-CT tomography

Micro-CT (Skyscan 1174, Bruker, Belgium) at 53 kV and 810 μA was used to scan the harvested femurs. The Inveon Research Workplace software (Siemens) was used for three-dimensional image reconstruction and quantification of the formed bone mass.

2.7.3. Histological analyses

The undecalcified femurs were dehydrated in an ascending ethanol gradient, embedded in methyl methacrylate resin, and sectioned using a microtome (310 CP, EXAKT, Germany). The sections were sanded and polished to a thickness of 50 μm for methylene blue-acid magenta staining (DB0088, Leagene Biotechnology, China). The BIOQUANT OSTEO 2019 system (BIOQUANT Image Analysis Corp, Nashville, TN, USA) was used to analyze the bone-to-implant contact (BIC) value and bone volume/total volume (BV/TV) ratio. Harvested femurs were desalted in EDTA decalcification solution, embedded in paraffin, and 5 μm thick horizontal sections were prepared for hematoxylin and eosin (H&E) and Masson staining.

2.8. RNA sequencing

HBMSCs were seeded at a density of 5×10^4 cells/mL on different specimens (Φ15 × 1.0 mm). Total cellular RNA was extracted on day 7 after osteogenic induction. Sequencing was performed using the Next-Generation Sequencing. Reads were mapped to the human genome (GRCh38). EdgeR was used to identify differentially expressed genes (DEGs). Genes with FPKM <0.1 in both the control and experimental group were ignored in the subsequent analysis. Gene Ontology (GO) and Kyoto Encyclopedia of Genes and Genomes (KEGG) were performed by R package cluster Profiler.

2.9. Statistical analysis

Data are expressed as mean ± standard deviation (SD). For parametric data, comparisons of different groups were performed using one-way analysis of variance, followed by Tukey's post hoc test for multiple comparisons. Statistical analyses were performed using GraphPad Prism 9 software (GraphPad Software Inc., San Diego, CA, USA). $P < 0.05$ was considered statistically significant.

3. Results

3.1. Characteristics of PEEK samples

The chloroauric acid solution was reduced using ascorbic acid to obtain AuNPs with a peak absorbance at approximately 520 nm, as determined by ultraviolet–visible spectroscopy (Fig. S1). The size range of AuNPs is about 10–30 nm, and the size of most AuNPs is approximately 15 nm. The surface morphology of the PEEK modified with AuNPs and metronidazole was observed using SEM (Fig. 1A). Compared to pure PEEK, the PEEK materials treated with metronidazole and AuNPs could be observed as a smooth coated film with visible protruding particles on the surface. There was no significant difference in surface morphology of different PEEK samples. In this study, dopamine was used as adhesive medium. Based on previous research and literature studies [27–29], dopamine may not possess significant antimicrobial ability and osteogenic activity. Although dopamine contributes to the photothermal effect of NIR light, a temperature above 60°C might be required to exhibit significantly antibacterial effect [30].

The surface roughness and hydrophilicity of different treated PEEK samples were shown in Fig. 1B and C. The results showed that the hydrophilicity of PEEK samples after surface treatment was significantly improved. The surface roughness of the PEEK samples treated with both AuNPs and metronidazole was increased, and the difference was statistically significant.

The results of elemental and semi-quantitative analyses by XPS (Fig. S2, Fig. 1E) showed that the appearance of nitrogen after surface treatment was related to the presence of metronidazole and dopamine in the PEEK coating. The AuNPs content in the PEEK coating was detected by ICP-MS. The content of AuNPs/P group was about 9.26 mg/L, which was approximately three times that of the M-AuNPs/P group (Fig. 1D). The catechol group played a central role in mimicking the adhesion properties of mussels. And the catechol mainly undergoes Michael addition and Schiff bases reactions with molecules containing amino or sulfhydryl groups. It can also undergo coordination reactions with metal ions [31,32]. In this study, metronidazole contained amino groups might first react with catechol group, meanwhile the AuNPs that coordinate with catechol group might be reduced.

3.2. Photothermal effects of PEEK samples surface

The characteristics of NIR light irradiation on the different PEEK

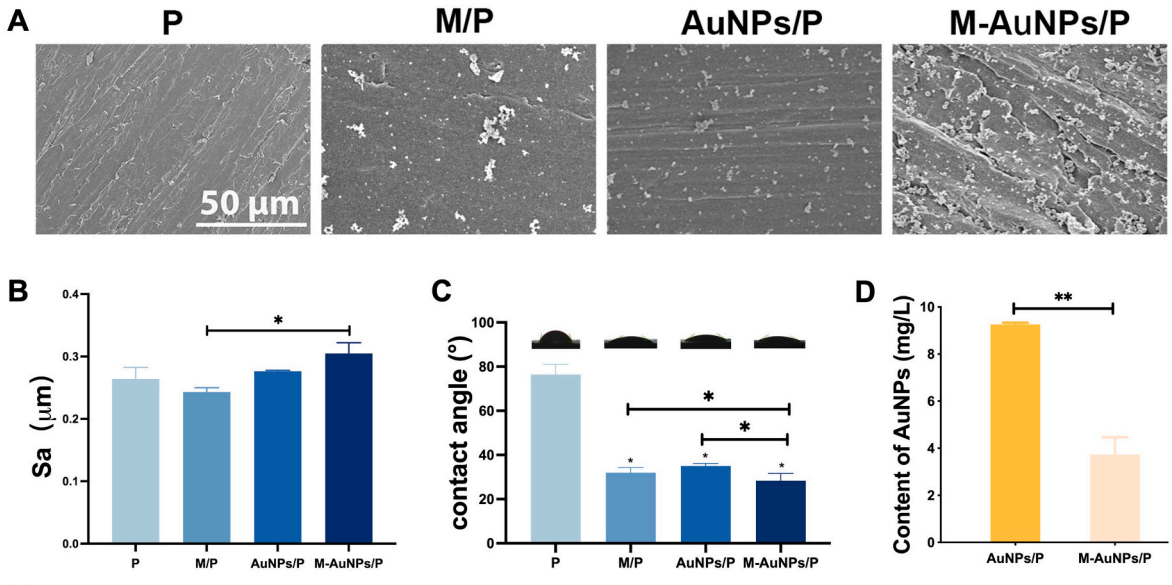

E

	C				N			O		
	C-C	C-O/C-N	C=O	O=C-O	Pyridinic N	Pyrrolic N	Pyridine-N-oxide	C=O/OH	C-O	H_2O ads
P	78.42	16.6	4.54	0.44	-	78.51	21.49	45.3	52.64	2.06
M/P	57.59	29.01	6.6	6.8	11.40	69.13	19.47	27.68	70.02	2.3
AuNPs/P	59.22	29.07	5.31	6.4	16.33	67.09	16.58	30.93	67.04	2.03
M-AuNPs/P	62.11	26.31	6.2	5.38	14.15	70.5	15.35	28.2	70.11	1.69

Fig. 1. The surface characteristics of different PEEK samples. (A) Surface morphology of different PEEK samples. (B) Roughness of different PEEK samples. *$P < 0.05$. (C) Water contact angle of different PEEK samples. *$P < 0.05$. (D) The content of AuNPs adhered on the AuNPs/P group and M-AuNPs/P group. **$P < 0.01$. (E) The ratio of chemical valence of different samples surface analyzed by XPS.

samples surface were shown in Fig. 2. After irradiation for 10 min, the temperature of the pure PEEK group increased by about 10°C, reaching a temperature below 35°C. This rise in temperature may be related to the fact that NIR light itself can be converted into heat energy. Particularly, the temperature of the treated PEEK groups increased significantly, reaching about 42°C. There was a significant difference between the PEEK group and the treated PEEK groups. The increase in temperature of the metronidazole coating suggested that polydopamine might contribute to the temperature rise [30] (Fig. 2B). AuNPs had a minor impact on the increase in temperature of the AuNPs coating. However, the thermal cycling curve of the PEEK samples treated without AuNPs showed that the temperature decreased to its original value after 14 min (Fig. 2C and D).

In addition, Fig. 2H depicted the release of AuNPs from different samples coating within 21 days. The results suggested that NIR may facilitate the release of AuNPs from the coating. Fig. 2G displayed the release of metronidazole from the coatings of different samples within 21 days. The released amount of metronidazole was greater when it was combined with AuNPs and the coating was stimulated by NIR light. The results showed that the release of AuNPs and metronidazole was related to the response of the coatings to NIR light. Moreover, the release of metronidazole was significantly correlated with the response of AuNPs to NIR light after three days. Therefore, the difference in release between the different groups may be mainly related to the response of AuNPs to NIR light. The AuNPs have good photothermal effects. In some studies of AuNPs loading drugs, the drug release could be achieved by thermally activated desorption and diffusion [33,34].

3.3. Antimicrobial properties of PEEK samples in vitro

Through WST detection and colony counting experiments at 24 h, we preliminarily explored the antibacterial effects of metronidazole and AuNPs coatings, and explored the possible effects of NIR light irradiation on bacterial viability. Pure PEEK materials had almost no effect on *P. gingivas* activity (Fig. 3) with or without NIR light irradiation. In contrast, the bacterial viability on the surface of metronidazole- and AuNPs-modified PEEK materials was significantly reduced. The antibacterial ability of AuNPs coating was slightly better than that of metronidazole coating, but there was no significantly difference *in vitro*.

The results of Fig. 2H showed that the amount of AuNPs in the AuNPs coating bounded with metronidazole was significantly reduced, and on the first day, the release of AuNPs in this coating was less than that of the AuNPs coating alone. However, the antibacterial effect of the AuNPs coating combined with metronidazole was significantly improved. In summary, each component individually could contribute to the antibacterial activity, and the combined use of AuNPs and metronidazole could significantly improve this effect.

Furthermore, the results of the live/dead staining of bacteria also exhibited the same trend (Fig. 3C), with green indicating living bacteria and red indicating dead bacteria. The antimicrobial effect on the surface

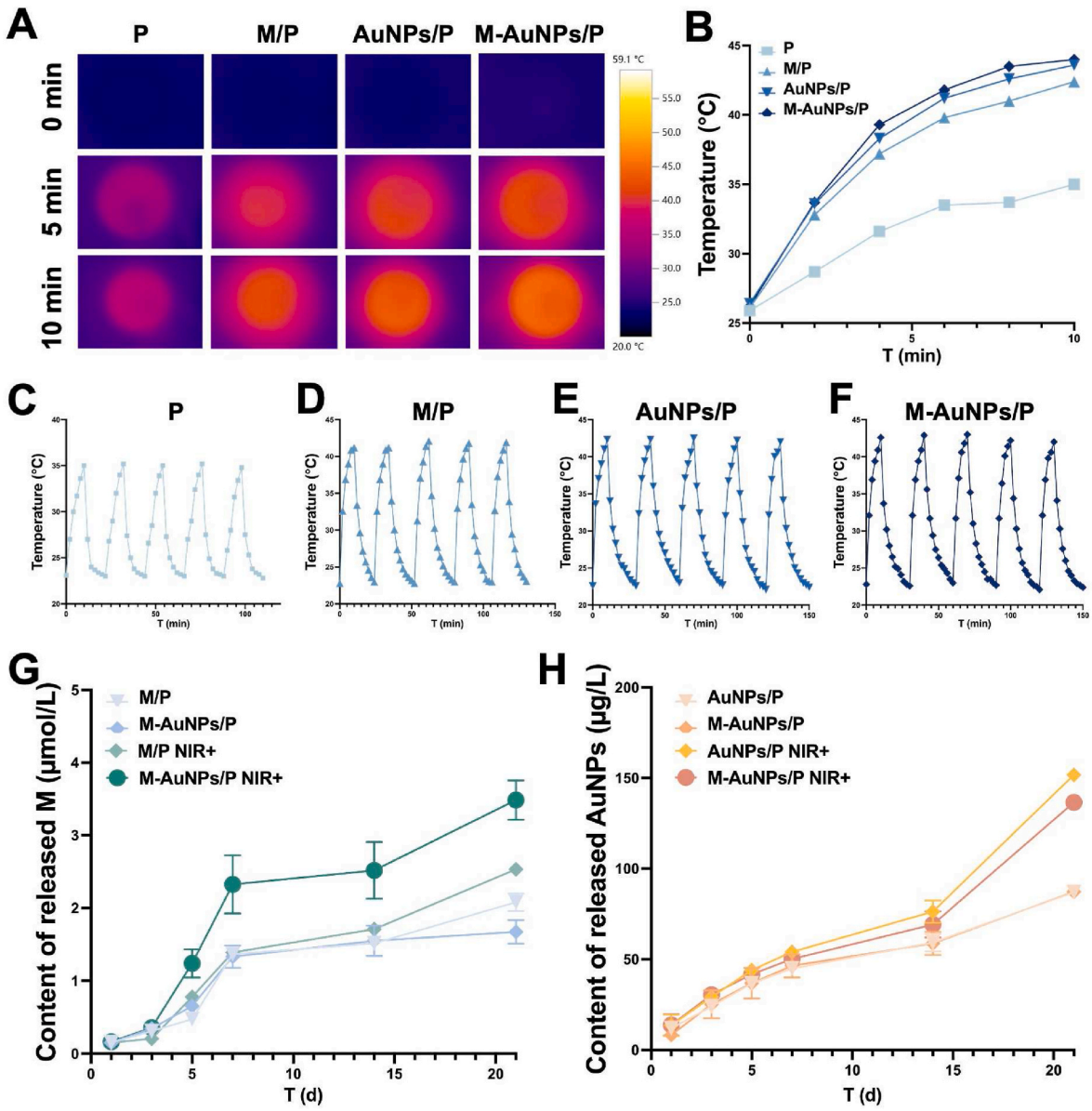

Fig. 2. Photothermal effects of different PEEK samples and the release of AuNPs and metronidazole from the PEEK coatings. (A) Thermal image of different samples. (B) Temperature change over time on the surface of different samples. (C) Thermal cycling curve of P group. (D) Thermal cycling curve of M/P group. (E) Thermal cycling curve of AuNPs/P group. (F) Thermal cycling curve of M-AuNPs/P group. (G) The content of metronidazole released from different samples coating within 21 days. (H) Release of AuNPs within 21 days in the coating of PEEK materials.

of the PEEK material modified by AuNPs combined with metronidazole was significantly improved. Due to the organization's inability to tolerate temperature exceeding about 45°C, *in vivo* osseointegration experiment was still being carried out under this NIR light condition.

3.4. Biocompatibility in vitro

The *in vitro* biocompatibility of the different PEEK samples was determined by observing the cell morphology, cytoskeleton, cell proliferation, and osteogenic differentiation of hBMSCs. And the biocompatibility of the different PEEK samples under NIR light was also elucidated. Fig. 4A–B showed the cell morphology and cytoskeleton of hBMSCs seeded on the surfaces of the different PEEK samples at 4 h and 24 h respectively. After cultured for 4 h, the cells on the surface of the pure PEEK specimen appeared clump-like, and the cytoskeleton was unclear. But the images of cell morphology on pure PEEK specimen under NIR light showed the irradiation of NIR light increased the area of cell expansion. Particularly, the cells on the surfaces of the treated PEEK groups were well spread and had significantly protruded pseudopodia. After 24 h of culture, although the cells on the pure PEEK surface extended, there were still a few pseudopodia. However, the cells on the treated PEEK surfaces exhibited abundant pseudopodia.

Cell proliferation was observed using CCK-8 assay after 1, 3, 5, and 7 days (Fig. 4C). All of the PEEK samples performed well in this assay. The expression of osteogenic genes and alizarin red staining (ARS) were evaluated to explore the osteogenic differentiation of HBMSCs on the different PEEK samples. The relative expression of alkaline phosphatase (*ALP*) and Collagen I genes demonstrated the early osteogenic differentiation. The results (Fig. 4D and E) showed that the genes expression of M-AuNPs/P group increased, and that further significantly increased after NIR light irradiation. The ARS staining demonstrated relatively late osteogenic differentiation. The results of ARS (Fig. 4F, Fig. S3) showed that osteogenic property on the surface of the PEEK samples treated by AuNPs and metronidazole was significantly improved. Furthermore,

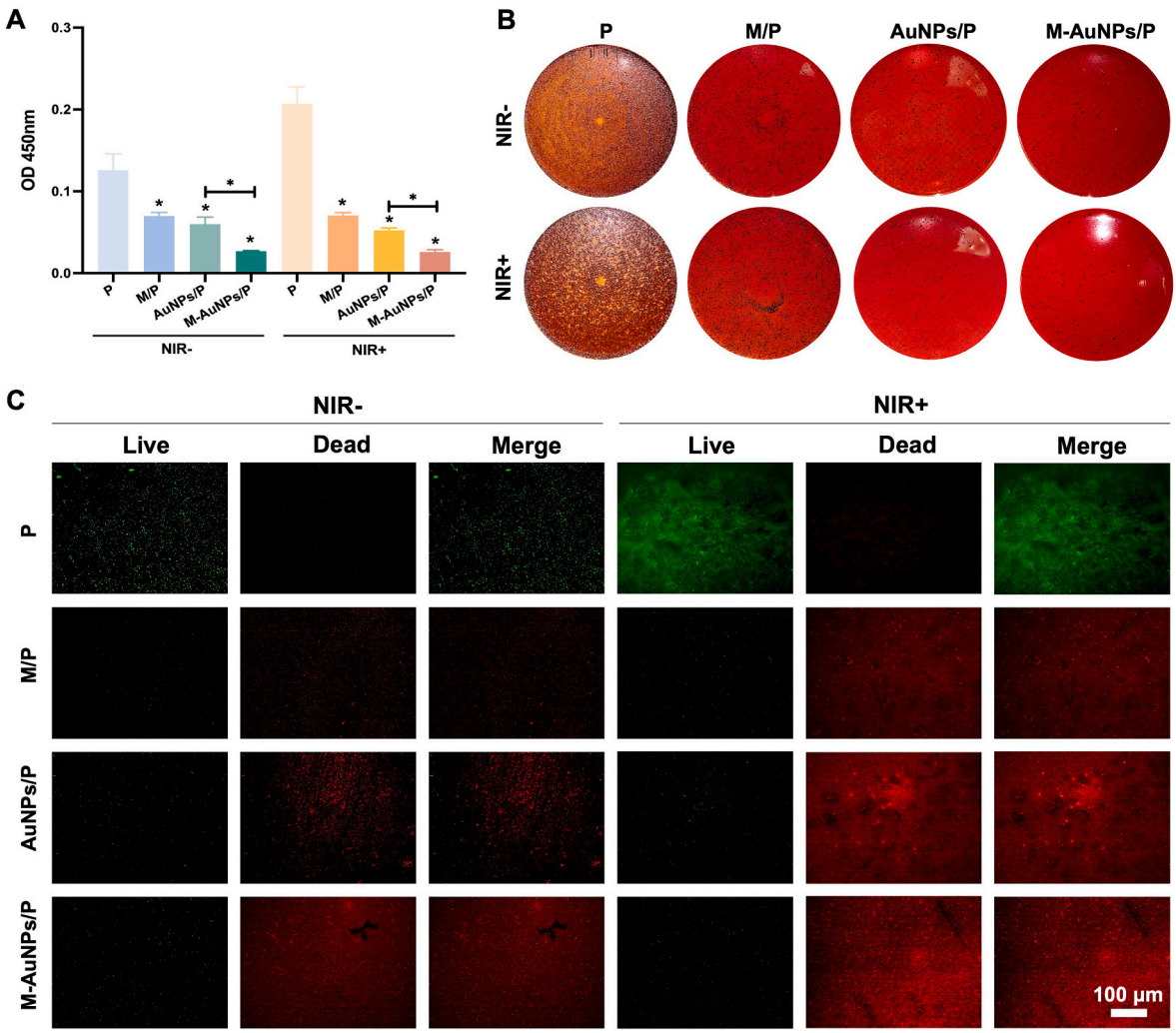

Fig. 3. Evaluation of antibacterial effect of the treated PEEK materials *in vitro*. (A) The WST assay of functionalized PEEK samples against Gram-negative *P. gingivalis* cultured for 24 h $^*P < 0.05$. (B) Colonies of functionalized PEEK samples in the blood agar plates. (C) Live/dead staining of bacteria on the surface of different PEEK specimens. Green: live bacteria, Red: dead bateria. (For interpretation of the references to colour in this figure legend, the reader is referred to the Web version of this article.)

NIR light irradiation could further promote bone formation.

3.5. Antimicrobial properties of PEEK samples in vivo

A subcutaneous implantation model on mice was used to evaluate the antibacterial effect of modified PEEK materials. The results were shown in Fig. 5. Fig. 5A showed the surface topography of different PEEK implants infected with bacteria after 3 days and 7 days *in vivo*. Fig. S4 showed the topography of a pure PEEK material without bacterial infection after implantation. The SEM images of the infected PEEK samples showed that the bacteria on the surface of the pure PEEK implants showed a short column with good morphology with or without light (yellow arrow). The *P. gingivalis* on the surface of the AuNPs coating combined with metronidazole were few and irregularly shaped. Moreover, the bacteria on the surface of the modified PEEK implants after NIR light irradiation were wrinkled.

The peri-implant tissues were collected for bacteria culture and staining with H&E (Fig. 5D), Masson (Fig. 5E), and Giemsa (Fig. 5F). The H&E staining was used to observe inflammatory cells (black triangle). Masson staining was used to analyze collagen fibers, And Giemsa staining was used to observe the number of bacteria (yellow arrow). The results showed that more inflammatory cells were still present in the surrounding tissues of pure PEEK implants at 7 days after implantation. However, fewer inflammatory cells were found in the surrounding tissues of M-AuNPs-modified PEEK implants and more fibroblasts were present in the surrounding tissues. Masson staining results showed a significant increase in collagen fibers in the surrounding tissues of M-AuNPs-modified PEEK implants compared to those around pure PEEK implants (red five-pointed star), and the NIR light further improved these effects at 7 days. Giemsa staining revealed the presence of a large number of bacteria in the tissue surrounding of the pure PEEK implants.

3.6. Osseointegration effect of PEEK samples in vivo

In vitro osteogenic activity assays showed that the surface of the PEEK materials modified with metronidazole and AuNPs and stimulated by NIR light significantly promoted osteogenesis compared with that of the pure PEEK. Moreover, the antibacterial results showed that both M-AuNPs/P and M-AuNPs/P (NIR+) groups exhibited excellent antibacterial effects. Therefore, P group, M-AuNPs/P group, and M-AuNPs/P (NIR+) group were chosen for *in vivo* experiments. The rat femoral model was used for investigating the osseointegration of PEEK. The surgical process of cylindrical PEEK implants implantation into the femoral and postoperative NIR irradiation are shown in Fig. 6A.

At 4 and 8 weeks after surgery, rat femurs were collected and analyzed using micro-CT and tissue section staining. Fig. 6B showed 2D-

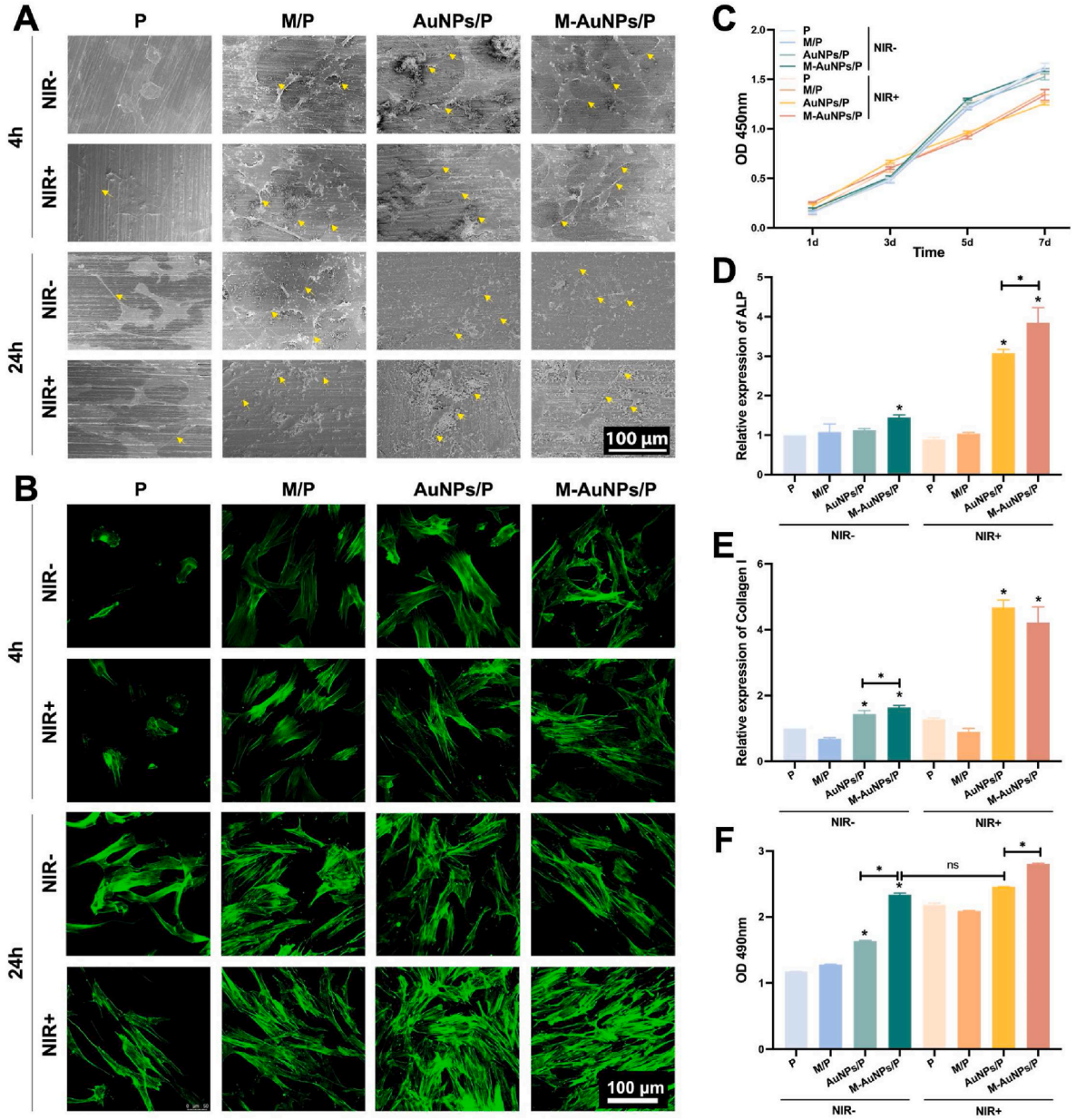

Fig. 4. Bioactivity of different PEEK samples *in vitro*. (A) Morphology of HBMSCs on the surface of different PEEK samples at 4 h and 24 h. The yellow arrows represent pseudopodia. (B)Cytoskeleton of HBMSCs on the surface of different PEEK samples at 4 h and 24 h. (C) Proliferation curve of HBMSCs. (D) Relative expression of osteogenic genes encoding *ALP*. $^*P < 0.05$. (E) Relative expression of osteogenic genes encoding Collagen I. $^*P < 0.05$. (F) Quantification analysis of alizarin red staining. $^*P < 0.05$. Ns, not significant. (For interpretation of the references to colour in this figure legend, the reader is referred to the Web version of this article.)

CT and 3D reconstruction images of the bone tissue that formed around the implanted PEEK materials in the bone marrow cavity. The yellow arrow indicated that the bone tissue around the implants was discontinuous, which was evident in the pure PEEK group. This observation reflects suboptimal bone growth around the pure PEEK implants, which indicates worse osseointegration. More bone tissue formation can be observed around the PEEK implants modified with AuNPs combined with metronidazole, and the thickness was approximately twice that of the pure PEEK group. NIR light irradiation could further promote the formation of trabeculae bone. BV/TV can directly reflect the amount of bone mass. Tb.Th reflects the average thickness of the trabecular bone. And Tb. Sp represents the average width of the medullary cavity between the trabeculae. Quantitative analyses of bone volume/total volume (BV/TV), trabecular thickness (Tb·Th), and trabecular separation (Tb.Sp) are shown in Fig. 6C-E. At 4 weeks, the BV/TV value of the M-AuNPs/P implants significantly increased than that of the pure PEEK group, and that of the M-AuNPs/P (NIR+) group was higher than that of the other groups. The Tb·Th results showed the same trend, whereas those of Tb. Sp showed the opposite trend. The results indicated that the coating of AuNPs combined with metronidazole was conducive to bone formation, and NIR light responsive coating could achieve better osteogenic effects. At 8 weeks, compared with the pure PEEK group, the osteogenic effects of the M-AuNPs/P group were more obvious, and there were statistical differences in BV/TV, Tb·Th, and Tb·Sp. Moreover, NIR irradiation showed advantages for bone formation.

3.7. Histological analysis

Uncalcified bone tissue sections were stained with methylene blue-acid magenta to observe bone formation around the implants at 4

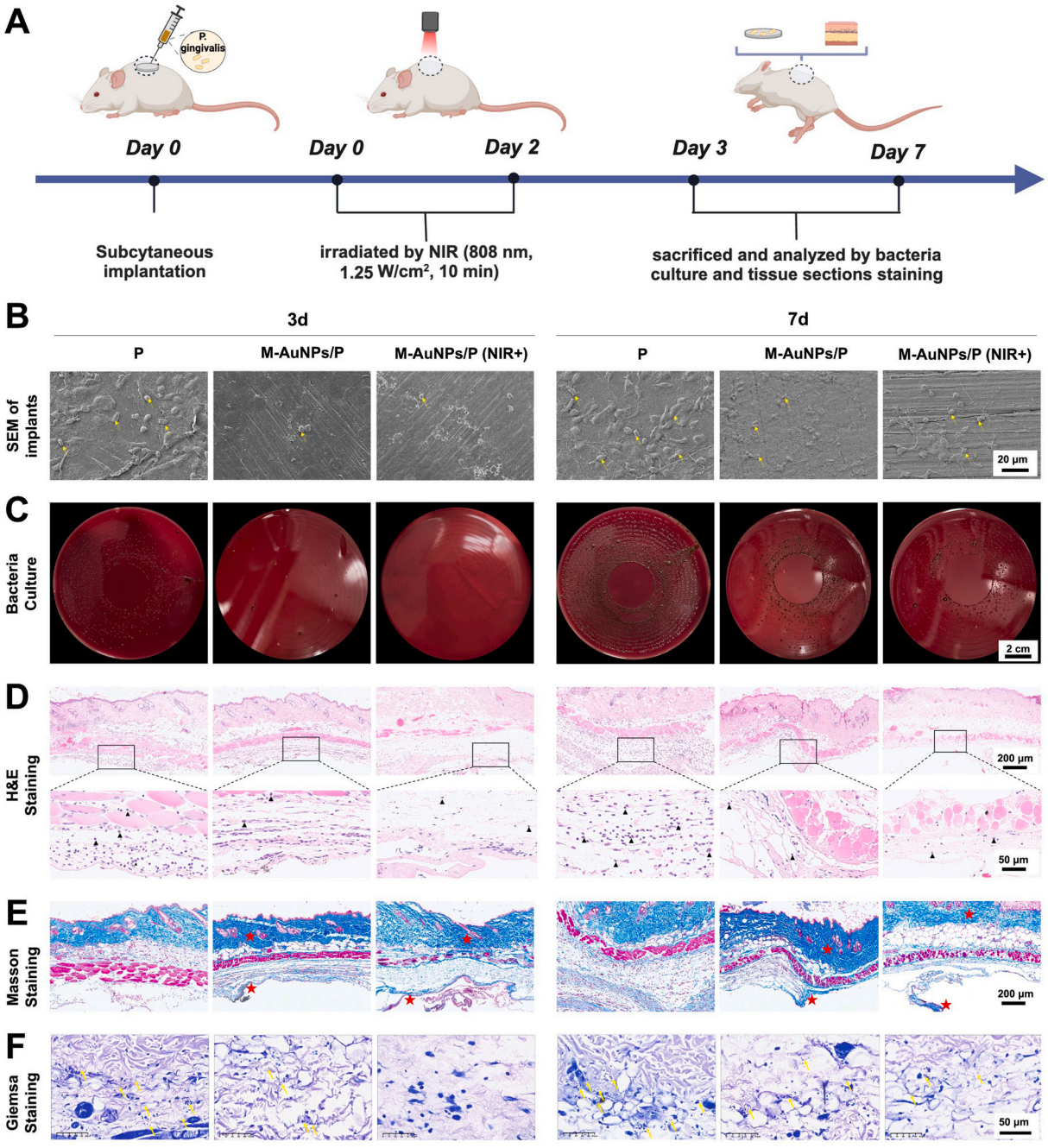

Fig. 5. Schematic diagram of subcutaneous implantation and evaluation of antibacterial effect of the treated PEEK materials with or without NIR irradiation *in vivo* at 3 days and 7 days. (A) Schematic diagram of subcutaneous implantation in BALB/c mice and NIR light irradiation. (B) The topography of different PEEK implants infected by bacteria *in vivo* (yellow arrows represent bacteria). (C) The culture of bacteria in the tissue surrounding different PEEK implants. (D) The H&E staining of the tissue surrounding different PEEK implants (black triangles represent inflammatory cells). (E) The Masson staining of the tissue surrounding different PEEK implants (red five-pointed stars represent collagen fibers). (F) The Giemsa staining of the tissue surrounding different PEEK implants (yellow arrows represent bacteria). (For interpretation of the references to colour in this figure legend, the reader is referred to the Web version of this article.)

weeks and 8 weeks (Fig. 7A). The green arrow showed the direct contact between the implants and bone tissue. Compared to the pure PEEK implants, more bone tissue contacted directly to the implants was observed around the treated PEEK implants. The bone-implant contact (BIC) is an important indicator used to evaluate the stability of dental implants [35]. At 4 weeks, the BIC value of the M-AuNPs/P group was significantly higher than that of the pure PEEK group (Fig. 7B). And the BIC value was about twice that of the pure PEEK group after NIR light irradiation, indicating that the coated PEEK implants with NIR light is more stable in rat femurs. At 8 weeks, the BIC value between pure PEEK implants and bone tissue did not show a significant increase compared to the BIC value of 4 weeks, with a BIC value of approximately 40%. However, the coated PEEK implants showed a significant increase in direct contact with surrounding bone tissue, with approximately 80% at 8 weeks. Additionally, the BIC value of M-AuNPs/P (NIR+) group had already reached 80% at 4 weeks after implantation (Fig. 7B). The results of bone volume analysis (Fig. 7C) and trabecular analysis (Fig. 7D and E) were basically consistent with those of Micro-CT.

The results of H&E staining and Masson staining (Fig. 8) also illustrated the influence of the surface modification on new bone formation.

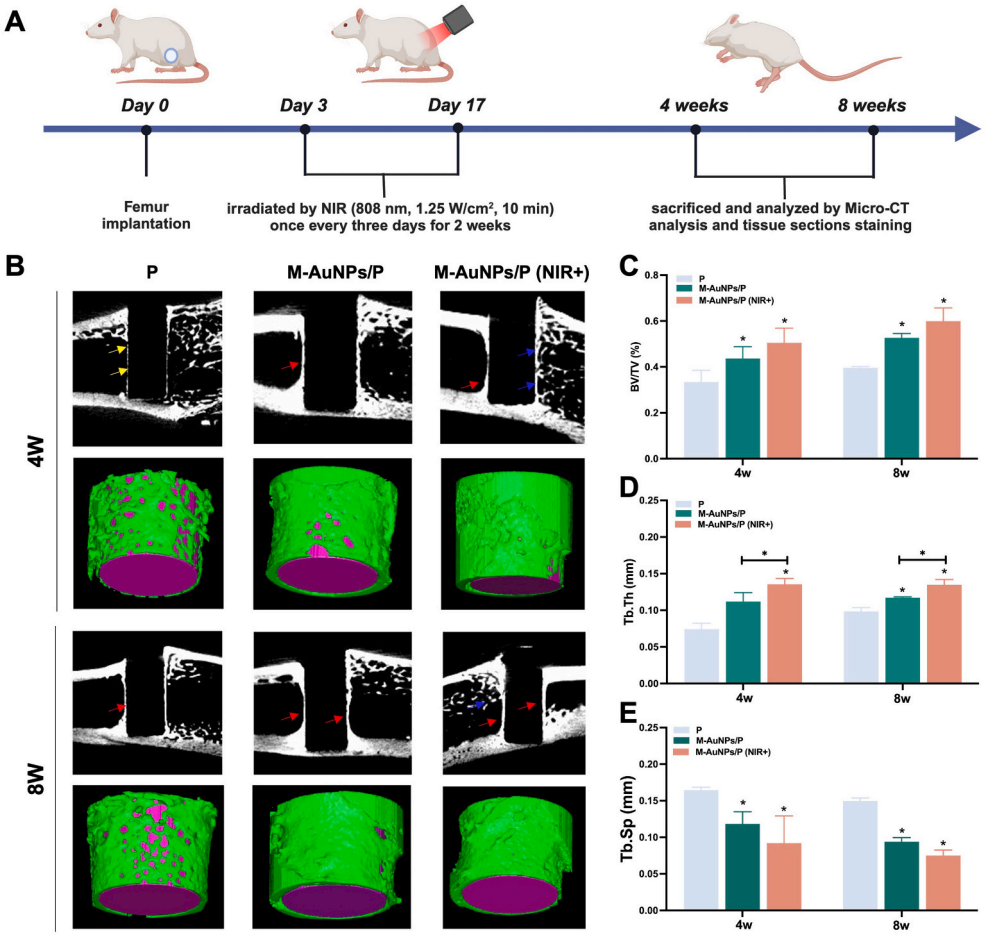

Fig. 6. Schematic diagram of rat femur implantation and Micro-CT analysis of different PEEK samples for *in vivo* bone formation. (A) Schematic diagram of rat femur implantation and NIR light irradiation. (B) 2D-CT and 3D reconstruction images of rat femur with implants after 4 and 8 weeks of implantation. The yellow arrow: areas of boneless tissue. The red arrow: bone tissue around the implant. The blue arrow: trabecular bone. (C–E) Quantitative analysis of the different samples after 4 and 8 weeks of implantation. $^*P < 0.05$ compared with the pure PEEK group. (For interpretation of the references to colour in this figure legend, the reader is referred to the Web version of this article.)

In H&E staining of pure PEEK group, there were relatively numerous discontinuous tissues surrounding the implants. In Masson staining, the portion dyed blue constituted collagen fibers, indicated by the yellow arrow. Certain regions within the collagen fibers stained as red, signifying the maturation of bone tissue as indicated by the red arrow. At 4 weeks, the bone tissue around the coated group was more mature than that of the pure PEEK group, and the area of bone tissue in M-AuNPs/P (NIR+) group was relatively large. At 8 weeks, the bone tissue surrounding all implants showed more mature, especially in the M-AuNPs/P (NIR+) group. In addition, the H&E staining of major organs (Fig. S6) did not showed abnormalities.

3.8. Gene expression profiling by RNA sequencing

Due to the biological inertness of PEEK material, bone tissue and PEEK material cannot form direct connection. The above results stated that the surface modification in this study promoted bone formation, and improved the osseointegration rate *in vivo*. In order to understand the mechanism of the surface modification strategy on the biological behavior of osteoblasts in the early stage, RNA sequencing was done (Fig. 9). Through genetic differential analysis, compared with pure PEEK, 33 genes were significantly upregulated and 36 genes were downregulated in the AM modified group (Fig. 9A). GO enrichment and KEGG enrichment analysis were performed on differentially expressed genes. The process of conducting GO and KEGG enrichment analyses on differentially expressed genes revealed that the top five enriched entries predominantly pertain to gene functions mainly included: cytokine-cytokine receptor interaction, and PI3K-AKT signaling pathway. The genes primarily involved in the cytokine-cytokine receptor interaction include: *TNFSF15*, *BMP8B*, *BMP6*, *NGFR*, *LEP*, *CCL5* (Fig. 9C). The genes primarily involved in the PI3K-AKT signaling pathway include: *ARTN*, *KDR*, *ITGA6*, *ANGPT2*, *COMP*, *NGFR* (Fig. 9C). The other important downregulated genes include: *ATP1A1*, *MT2A*, *MT1E* (Fig. 9C), which were related to mineral absorption. Comparing M-AuNPs/P (NIR+) sample and M-AuNPs/P sample demonstrated the effects of NIR responsive coating on the gene expression of osteoblasts. Fig. 9B showed 21 genes were significantly upregulated and 11 genes were downregulated. GO enrichment analysis indicated seven significant differential expression genes: *BMP8B*, *LGI4*, *EGR3*, *ETV1*, *CHI3L1*, *WNT5A*, *LEP* (Fig. S7D). KEGG enrichment analysis indicated four significant differential expression genes: *LEP*, *HAAO*, *WNT5A*, *BMP8B* (Fig. 9D). Through analysis of differential genes and signaling pathways, the P13K-AKT signaling pathway may be the most essential, the mechanism of osteogenic differentiation of hBMSCs is as shown in Fig. 9E.

4. Discussion

The osseointegration of the implants in bone tissue is particularly important for stability of medical implants, especially dental or bone-defect repair implants [36]. The biological inertness of PEEK material

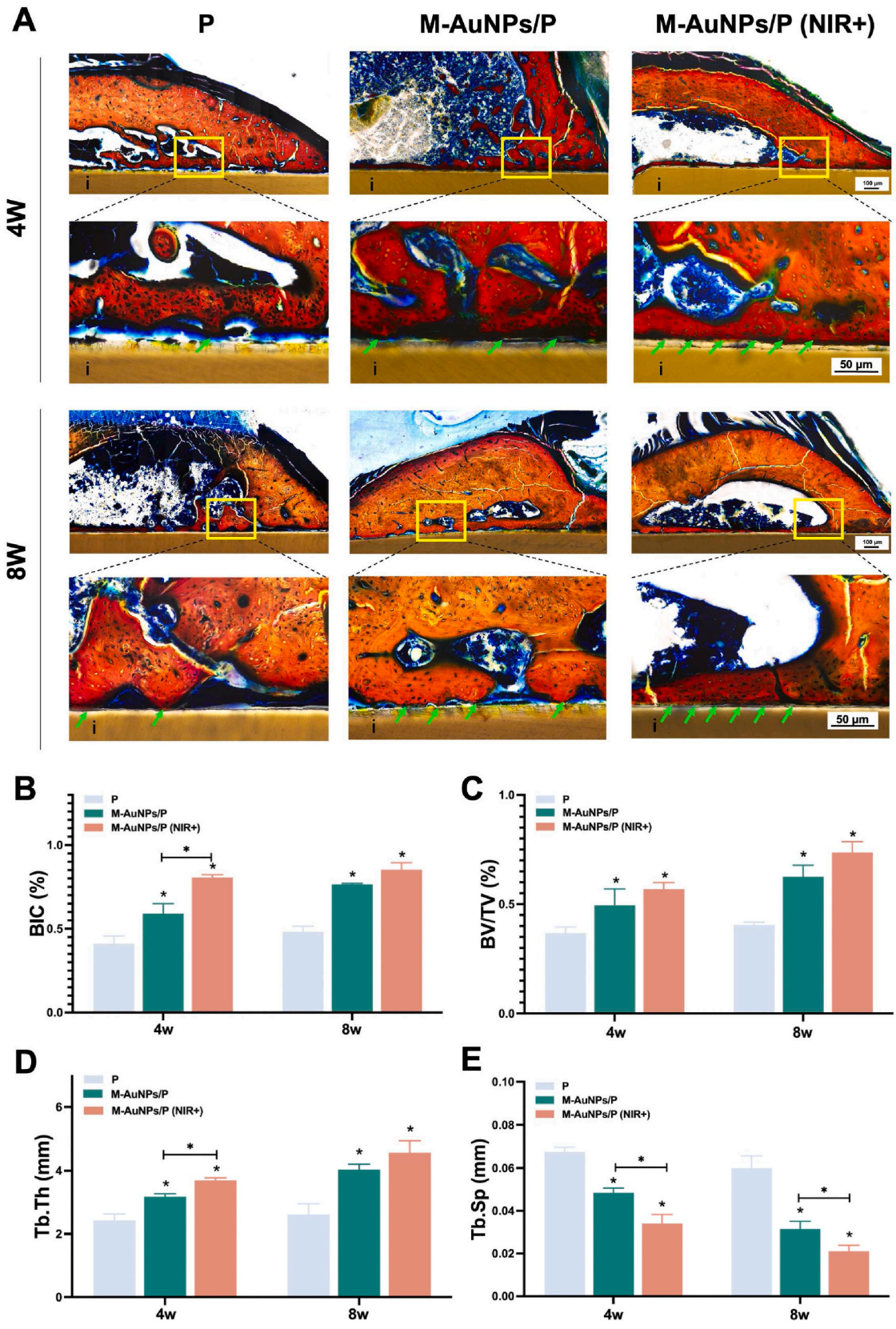

Fig. 7. Bone morphology analysis of different PEEK samples for *in vivo* bone formation at 4 weeks and 8 weeks. (A) Methylene blue-acid magenta staining of uncalcified bone tissue sections. i: implant. The green arrow represents the contact position between the implant and bone tissue. (B) Bone-to-implant contact of different PEEK samples *in vivo* bone formation. $^*P < 0.05$. (C) The BV/TV value analyzed by bone morphology analysis. (D) The trabecular thickness of different samples. $^*P < 0.05$. (E) The trabecular spacing of different samples. $^*P < 0.05$. (For interpretation of the references to colour in this figure legend, the reader is referred to the Web version of this article.)

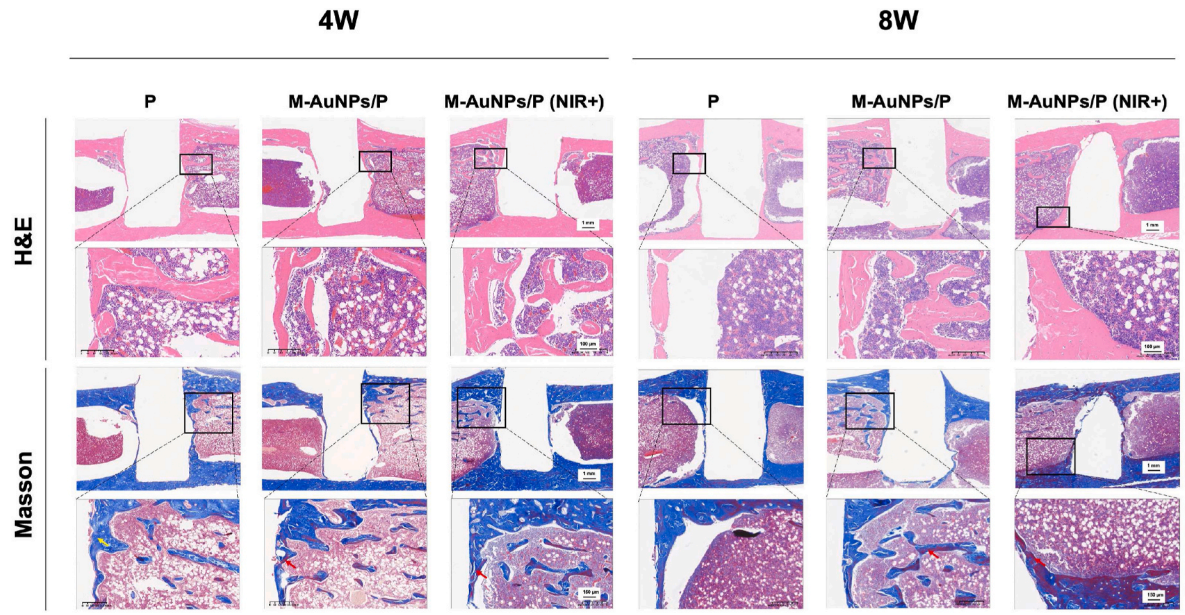

Fig. 8. Histological analysis of different PEEK samples for *in vivo* bone formation at 4 weeks and 8 weeks. H&E staining and Masson staining of different PEEK sample bone tissue sections.

limits its clinical use in dental implants. Surface modification is a potentially effective strategy for changing the surface characteristics and enhancing biological activity of PEEK materials [37,38]. Studies on the biological activity of pure PEEK have shown that peripheral bone formation around PEEK implants would be delayed, and the bone-implant contact of PEEK material with bone tissue was poor [4,39]. In addition, the antibacterial ability of pure PEEK was particularly weak [39]. Therefore, it is necessary to develop antibacterial and osteogenic properties for PEEK materials.

In this study, AuNPs coating combined with metronidazole effectively improved the antibacterial ability of the PEEK material, and the NIR light responsive AuNPs coating significantly enhanced the osseointegration of the PEEK implants. In the process of modification, polydopamine could enable the loading of functional molecules [40], includes many functional groups [41], such as planar indole units, amino groups, carboxylic acid groups, catechol or quinone functional groups, and indolic/catecholic systems for adhesion. The appearance of O–C═O chemical bonds and nitrogen element in the XPS results (Fig. 1E) might indicate that the polydopamine was adhered on the PEEK material. In addition, metronidazole and AuNPs were detected to successfully adhered into the PEEK coating by High-Performance Liquid Chromatography (HPLC) and Inductively Coupled Plasma-Mass Spectrometry (ICP-MS). The SEM images in Fig. 1A showed that polydopamine coating adhered to the PEEK surface. Polydopamine was also shown to be adhesive medium on the surfaces of experimental specimens in some studies [42,43]. What's more, all the coatings significantly improved the hydrophilicity of PEEK material, which could promote the adhesion of biomolecules and cells [44]. Cell adhesion is crucial in cellular communication and regulation, as well as in the development of tissues [45]. By observing the cells morphology and cytoskeleton, the pseudopodia of cells on the surfaces of coated PEEK materials were particularly obvious.

Research has showed that polydopamine has no obvious antibacterial effect [30]. In this study, the antibacterial effects of metronidazole and AuNPs adhered into PEEK coatings, as well as the released metronidazole and AuNPs, were evaluated. Bacterial adhesion to the device surface is the first and critical step in the pathogenesis of implant related infections [46]. The results showed that the AuNPs coating of the PEEK materials exhibited excellent antibacterial ability on the first day, which was similar to antibacterial ability of the metronidazole coating. The cell wall of gram-negative bacteria is thinner. The AuNPs could traverse the bacterial outer membrane peptidoglycan layer, thereby generating reactive oxygen species (ROS) and causing enzyme inactivation [47]. Moreover, after entering into bacteria, the AuNPs reduced adenosine triphosphate (ATP) levels and led to decreased metabolism [48,49]. In addition, AuNPs could target specific bacteria for exerting antibacterial effects by binding the specific functional molecules [22,23,50]. As shown in the antibacterial results of this study, compared with AuNPs coating and metronidazole coating, the antibacterial effects of AuNPs coating combined with metronidazole were further improved significantly. In addition to the functionalization of nanoscale gold particles could improve its antibacterial ability, the concentration of nanoscale gold particles and the types of bacteria might affect the antibacterial ability of nanoscale gold particles [21]. One study [51] showed that gold nanorods with a concentration of 8 μg/L have a significant antibacterial effects on *Staphylococcus aureus*. This study demonstrated that approximately 10 μg/L of AuNPs were released on the first day. The activity of *P. gingivalis* was significantly inhibited, and no significant cytotoxicity was observed. Ellen E et al. [19] thought the gold nanoparticles preparations with citrate and biotin did not appear to be toxic at concentrations up to 250 μM. What's more, AuNPs and metronidazole were found to continuously release within 21 days in this study. The cumulative amount of release was increased under NIR light after 21 days. Furthermore, the total release of metronidazole was significantly increased after binding to AuNPs under NIR light in 21 days. The results of *in vivo* experiments showed that the antibacterial effect of treated PEEK implants improved under NIR irradiation.

The stability of implants was related with good osseointegration. Bacterial infection and immune inflammation generally begin at the early stages of implantation into bone tissue of implants. The inhibition of infection and inflammation was beneficial for the bone formation on the surface of implant materials. Study indicated that gold nanoparticles can protect the growth plate against inflammatory damage by maintaining cartilage homeostasis [52]. Additionally, they can induce polarization of M2 macrophages [20], which is beneficial for bone formation. In this study, the osteogenic activity of coated PEEK materials *in vitro* was explored. The AuNPs coating combined with metronidazole have shown advantages in promoting osteogenesis. Fig. 1B and C demonstrated that the roughness of this coating was higher compared to the other groups and the hydrophilicity was better, which were related

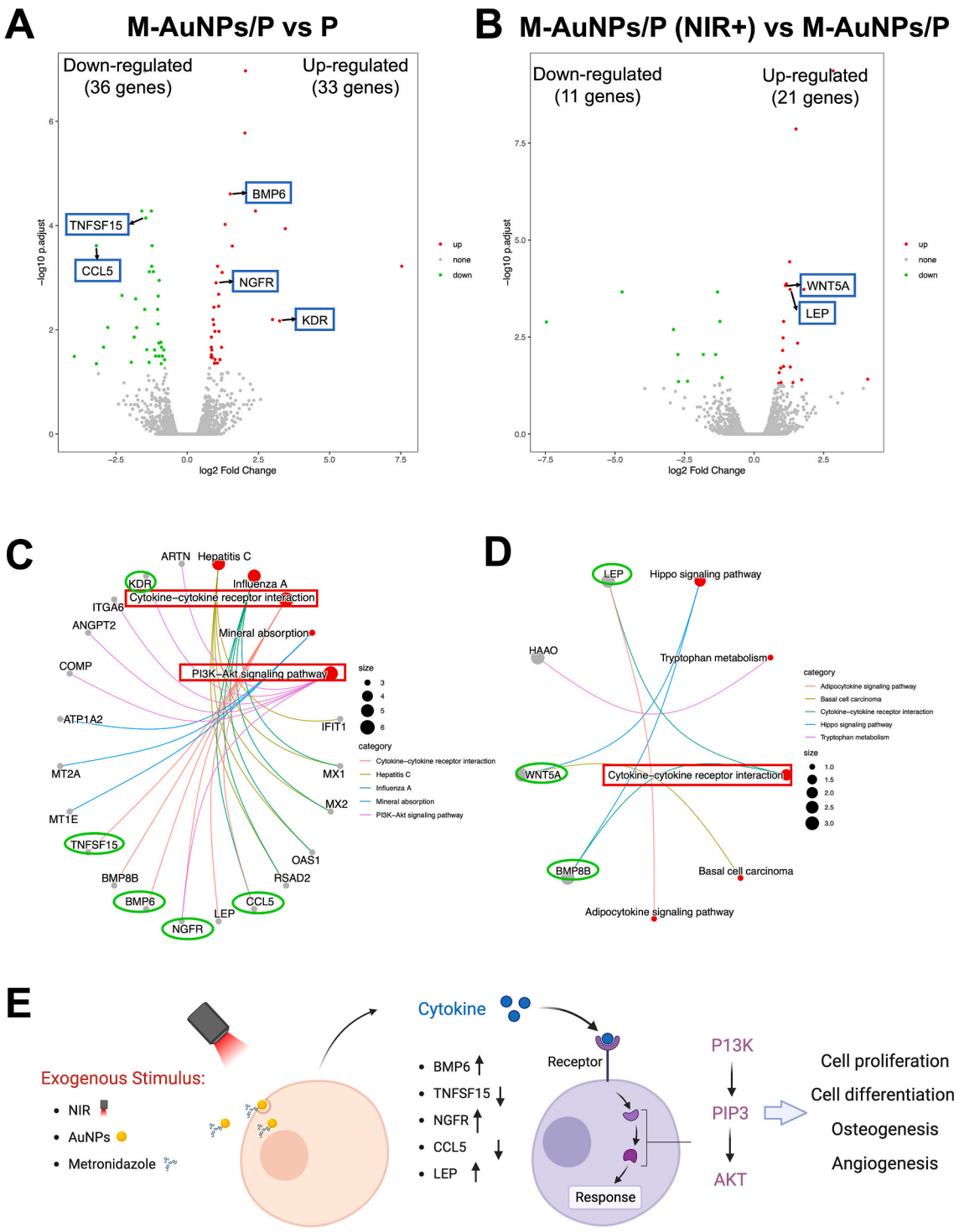

Fig. 9. Gene expression analysis of hBMSCs on P group, M-AuNPs/P group, and M-AuNPs/P (NIR+) group specimens. (A, C) RNA-seq analysis of M-AuNPs/P vs P. (B, D) RNA sequencing analysis of M-AuNPs/P (NIR+) vs M-AuNPs/P. (A) Volcano plot of significantly up-regulated ($p$value < 0.05) and down-regulated ($p$value < 0.05) genes in M-AuNPs/P group. Green dots: significantly down-regulated genes. Red dots: significantly up-regulated genes; Grey dots: not significantly up or down-regulated genes. (B) Volcano plot of significantly up-regulated ($p$value < 0.05) and down-regulated ($p$value < 0.05) genes in M-AuNPs/P (NIR+) group. (C) KEGG enrichment map of significantly regulated genes of M-AuNPs/P group enriched in the top five terms. (D) KEGG enrichment map of significantly regulated genes of M-AuNPs/P (NIR+) group enriched in the top five terms. (E) The mechanism for improving the osteogenic activity of HBMSCs on the treated PEEK samples. (For interpretation of the references to colour in this figure legend, the reader is referred to the Web version of this article.)

to osteogenesis [44]. After NIR light irradiation, the osteogenic activity of coated PEEK materials by AuNPs *in vitro* was significantly developed. Fig. 2H showed that more AuNPs were released under NIR light irradiation. Moreover, under NIR light, the content of AuNPs endocytosed into cells increased significantly (Fig. S8). In addition, the amount of AuNPs bound to metronidazole was also relatively higher. Gold nanoparticles have been shown to be effective in promoting osteogenesis at the right concentration and size [20,53,54]. A previous study indicated that the cellular uptake of AuNPs could be regulated by changes in their charge [55]. What's more, Metronidazole could suppress the production of

proinflammatory cytokines and exhibit immunoregulatory effects [56,57].

The photothermal phenomena of different PEEK samples were observed using thermal imager (Fig. 2). The surface heating effect of PEEK materials after dopamine bounded metronidazole treatment was obvious, and the temperature change of PEEK materials with AuNPs coating was slightly higher than that of PEEK materials with metronidazole coating. Moreover, the addition of AuNPs may be more conducive to maintaining the temperature of PEEK materials surface. What's more, the metronidazole combined to AuNPs could be more effectively released from the coating under NIR light irradiation. Particularly, NIR light could travel at least 10 cm through breast tissue and 4 cm through skull/brain tissue or deep muscle using microwatt laser sources [58]. Therefore, NIR light could respond to the surface coating of implants in rat femur [59,60]. In terms of safety, temperatures below 45°C typically do not cause irreversible damage to body tissues, and one study pointed out that about 42°C may be conducive to new bone formation [61]. In this study, the temperature of the treated PEEK samples rose to about 42°C (Fig. 2B), which met our requirements. Chen et al. [62] concluded that mild heat induces earlier differentiation of human mesenchymal stem cell (HMSC) and enhances the maturation of osteoblasts differentiated from HMSCs. Furthermore, Kunihiro Ikuta et al. [63] reported that a heat stimulus accelerates osteogenesis *in vivo*. Our results showed that the NIR light responsive AuNPs coating combined metronidazole had good osseointegration. Previous study [64] showed that the osteogenic effect of the pure PEEK under NIR was not significant. The use of NIR light is a relatively simple, safe, and effective strategy for improving osteogenesis through interaction with the AuNPs coating combined metronidazole.

The enhanced osteogenesis of treated PEEK materials [5,65,66] and NIR responsive PEEK materials was studied. In this study, the differential expression genes of hBMSCs on the surface of treated PEEK materials can be explained as the mechanism for enhanced osteogenesis. RNA sequencing data analysis was used to investigate the mechanism. Compared to the pure PEEK group, the differential expressed genes of top five enriched entries in the M-AuNPs/P group associated with the osteogenic mechanism are *LEP*, *BMP6* [67], *NGFR*, and *ATP1A2*, while those associated with angiogenesis are *KDR*. The downregulation of *TNFSF15* and *CCL5* genes indicates that this modification approach may also impact cellular immune processes. One study [68] showed that the osteogenesis of treated materials was improved by upregulation of *LEP* genes in BMSCs. And *LEP* was also able to regulate the inflammation of wound disorders and promote wound healing [69]. *BMP6* could modulate VEGF-induced endothelial cell sprouting by regulating expression of tip cell associated genes *VEGFR2 (KDR)* [70]. *NGFR* is the key receptor in neuronal growth and regeneration [71]. *ATP1A2* can exert its effect through the ERK1/2 signaling pathway [72]. The upregulation of *ATP1A2* gene [73] indicated that the response of bone marrow stromal cells to nanotubes may be mediated by the pathways previously implicated in transducing mechanical stress signals. The *TNFSF15* and *CCL5* genes played a promoting role in the inflammatory process [74]. In this study, the *TNFSF15* and *CCL5* genes exhibited a downregulation trend. It is worth noting that in addition to being associated with cell differentiation and angiogenesis [75], up-regulation of the *MT1E* gene may affect drug resistance [76].

Under NIR, changes in the *MT1E* gene are not significant, while the *MT2A* gene was significantly up-regulated. The *MT2A* gene was not included in the top five entries. The role of up-regulation of the *MT2A* gene included alleviating metal-induced toxicity [77]. One study [78] have shown that the *RSAD2* gene was significantly upregulated in M1 macrophages, promoting inflammation. In the M-AuNPs/P (NIR+) group of this study, the results showed that the *RSAD2* gene was significantly downregulated. The *WNT5A* gene has been demonstrated to induce M2 polarization of macrophages [79]. In this study, the surface temperature of the modified PEEK materials under NIR light rose to about 42°C. Research on the mechanism of promoting osteogenesis of mild heat stated that heat shock protein 70 (HSP70) could been significantly upregulated by mild heat shock [62,80], which has a direct effect on the differentiation of hMSCs into osteoblasts. It has also been shown that the expression levels of Wnt family member 5A (*WNT5A*), an important component of BMP2-mediated osteogenesis, are more abundant with NIR light exposure [81]. In this study, RNA sequencing data mining results showed that the *WNT5A* gene expression in the NIR-responsive group was up-regulated. On the one hand, they can secrete relevant cytokines to activate the P13K-AKT signaling pathway in osteoblasts, thereby improving osteogenic and angiogenic performance. On the other hand, the expression of osteogenesis-related genes indicated the promotion of bone formation. Through RNA sequencing analysis, we revealed the potential underlying mechanism of promoting bone formation with the coating. This served as a foundation for further in-depth mechanism research.

5. Conclusion

A safer, simple, and feasible surface modification method was developed and can effectively adhere metronidazole and AuNPs to the surface of PEEK materials. After the surface modification, the antibacterial ability and osteogenic activity of PEEK were enhanced. NIR light irradiation played a positive role in osseointegration for the AuNPs coating combined metronidazole on the PEEK implants. The coating may primarily affect the inflammatory response, modulating the release of cytokines, and promoting bone formation through active the P13K-AKT signaling pathway. The NIR light-responsive drug-loaded AuNPs coating is a potential strategy that endows PEEK with enhanced osseointegration and antibacterial properties.

CRediT authorship contribution statement

Xinxin Zhan: Conceptualization, Data curation, Investigation, Methodology, Writing – original draft, Writing – review & editing. **Jianglong Yan:** Conceptualization, Resources. **Dong Xiang:** Methodology, Software. **Hao Tang:** Methodology, Software. **Lulu Cao:** Methodology, Software. **Yufeng Zheng:** Conceptualization, Resources. **Hong Lin:** Formal analysis, Supervision, Writing – review & editing. **Dandan Xia:** Formal analysis, Supervision, Writing – review & editing.

Declaration of competing interest

The authors declare that they have no known competing financial interests or personal relationships that could have appeared to influence the work reported in this paper.

Data availability

Data will be made available on request.

Appendix A. Supplementary data

Supplementary data to this article can be found online at https://doi.org/10.1016/j.mtbio.2024.100982.

References

[1] X. Wang, K. Zhou, Y. Li, H. Xie, B. Wang, Preparation, modification, and clinical application of porous tantalum scaffolds, Front. Bioeng. Biotechnol. 11 (2023) 1127939.
[2] H. Ma, A. Suonan, J. Zhou, Q. Yuan, L. Liu, X. Zhao, X. Lou, C. Yang, D. Li, Y.-g. Zhang, PEEK (Polyether-ether-ketone) and its composite materials in orthopedic implantation, Arab. J. Chem. 14 (3) (2021).
[3] S.M. Kurtz, J.N. Devine, PEEK biomaterials in trauma, orthopedic, and spinal implants, Biomaterials 28 (32) (2007) 4845–4869.
[4] F.P. Koch, D. Weng, S. Kramer, S. Biesterfeld, A. Jahn-Eimermacher, W. Wagner, Osseointegration of one-piece zirconia implants compared with a titanium implant

of identical design: a histomorphometric study in the dog, Clin. Oral Implants Res. 21 (3) (2010) 350–356.
[5] A. Gao, Q. Liao, L. Xie, G. Wang, W. Zhang, Y. Wu, P. Li, M. Guan, H. Pan, L. Tong, P.K. Chu, H. Wang, Tuning the surface immunomodulatory functions of polyetheretherketone for enhanced osseointegration, Biomaterials 230 (2020) 119642.
[6] A. Wiessner, T. Wassmann, J.M. Wiessner, A. Schubert, B. Wiechens, T. Hampe, R. Burgers, In Vivo biofilm formation on novel PEEK, titanium, and zirconia implant abutment materials, Int. J. Mol. Sci. 24 (2) (2023).
[7] Z. Zheng, P. Liu, X. Zhang, X. Jingguo, W. Yongjie, X. Zou, X. Mei, S. Zhang, S. Zhang, Strategies to improve bioactive and antibacterial properties of polyetheretherketone (PEEK) for use as orthopedic implants, Mater Today Bio 16 (2022) 100402.
[8] L. Abusleme, A. Hoare, B.Y. Hong, P.I. Diaz, Microbial signatures of health, gingivitis, and periodontitis, Periodontol 86 (1) (2021) 57–78, 2000.
[9] A.P.V. Colombo, A.C.R. Tanner, The role of bacterial biofilms in dental caries and periodontal and peri-implant diseases: a historical perspective, J. Dent. Res. 98 (4) (2019) 373–385.
[10] S. Lofmark, C. Edlund, C.E. Nord, Metronidazole is still the drug of choice for treatment of anaerobic infections, Clin. Infect. Dis. 50 (Suppl 1) (2010) S16–S23.
[11] A. Mombelli, Microbial colonization of the periodontal pocket and its significance for periodontal therapy, Periodontol 76 (1) (2018) 85–96, 2000.
[12] M. Reise, R. Wyrwa, U. Muller, M. Zylinski, A. Volpel, M. Schnabelrauch, A. Berg, K.D. Jandt, D.C. Watts, B.W. Sigusch, Release of metronidazole from electrospun poly(L-lactide-co-D/L-lactide) fibers for local periodontitis treatment, Dent. Mater. 28 (2) (2012) 179–188.
[13] M.H. Ho, H.C. Chang, Y.C. Chang, J. Claudia, T.C. Lin, P.C. Chang, PDGF-metronidazole-encapsulated nanofibrous functional layers on collagen membrane promote alveolar ridge regeneration, Int. J. Nanomed. 12 (2017) 5525–5535.
[14] M.C. Bottino, V. Thomas, G.M. Janowski, A novel spatially designed and functionally graded electrospun membrane for periodontal regeneration, Acta Biomater. 7 (1) (2011) 216–224.
[15] C. Alauzet, A. Lozniewski, H. Marchandin, Metronidazole resistance and nim genes in anaerobes: a review, Anaerobe 55 (2019) 40–53.
[16] M. Ramstedt, B. Ekstrand-Hammarström, A.V. Shchukarev, A. Bucht, L. Osterlund, M. Welch, W.T. Huck, Bacterial and mammalian cell response to poly(3-sulfopropyl methacrylate) brushes loaded with silver halide salts, Biomaterials 30 (8) (2009) 1524–1531.
[17] K. Mijnendonckx, N. Leys, J. Mahillon, S. Silver, R. Van Houdt, Antimicrobial silver: uses, toxicity and potential for resistance, Biometals 26 (4) (2013) 609–621.
[18] H. Daraee, A. Eatemadi, E. Abbasi, S. Fekri Aval, M. Kouhi, A. Akbarzadeh, Application of gold nanoparticles in biomedical and drug delivery, Artif. Cells, Nanomed. Biotechnol. 44 (1) (2016) 410–422.
[19] E.E. Connor, J. Mwamuka, A. Gole, C.J. Murphy, M.D. Wyatt, Gold nanoparticles are taken up by human cells but do not cause acute cytotoxicity, Small 1 (3) (2005) 325–327.
[20] W. Peilin, P. Ying, W. Renyuan, L. Zhuoxuan, Y. Zhenwu, Z. Mai, S. Jianguo, Z. Hao, Y. Gang, L. Lin, L. Haodong, Size-dependent gold nanoparticles induce macrophage M2 polarization and promote intracellular clearance of Staphylococcus aureus to alleviate tissue infection, Mater Today Bio 21 (2023) 100700.
[21] X. Gu, Z. Xu, L. Gu, H. Xu, F. Han, B. Chen, X. Pan, Preparation and antibacterial properties of gold nanoparticles: a review, Environ. Chem. Lett. 19 (1) (2020) 167–187.
[22] X. Zhao, H. Tang, X. Jiang, Deploying gold nanomaterials in combating multi-drug-resistant bacteria, ACS Nano, 16 (7) (2022) 10066–10087.
[23] A. Mohammed Fayaz, M. Girilal, S.A. Mahdy, S.S. Somsundar, R. Venkatesan, P. T. Kalaichelvan, Vancomycin bound biogenic gold nanoparticles: a different perspective for development of anti VRSA agents, Process Biochem. 46 (3) (2011) 636–641.
[24] R. Vankayala, K.C. Hwang, Near-infrared-light-activatable nanomaterial-mediated phototheranostic nanomedicines: an emerging paradigm for cancer treatment, Adv. Mater. 30 (23) (2018) e1706320.
[25] K. Deng, C. Li, S. Huang, B. Xing, D. Jin, Q. Zeng, Z. Hou, J. Lin, Recent progress in near infrared light triggered photodynamic therapy, Small 13 (44) (2017).
[26] Q. Feng, X. Zhou, C. He, NIR Light-Facilitated Bone Tissue Engineering, Wiley Interdiscip Rev Nanomed Nanobiotechnol, 2023 e1925.
[27] S. He, C. Duan, S. Wang, Y. Yu, Y. Kei Chan, X. Shi, J. Huang, S. Wang, S. Peng, Y. Deng, Fusion peptide-engineered polyetheretherketone implants with photo-assisted anti-pathogen and enhanced angiogenesis for in vivo osseointegrative fixation, Chem. Eng. J. 446 (2022).
[28] H. Ma, H. Han, X. Zhao, J. Ma, X. Qu, X. Lou, A. Suonan, B. Lei, Y. Zhang, Engineering multifunctional polyether ether ketone implant: mechanics-adaptability, biominerialization, immunoregulation, anti-infection, osteointegration, and osteogenesis, Adv. Healthcare Mater. 12 (12) (2023) e2202799.
[29] X. Xu, Y. Li, L. Wang, Y. Li, J. Pan, X. Fu, Z. Luo, Y. Sui, S. Zhang, L. Wang, Y. Ni, L. Zhang, S. Wei, Triple-functional polyetheretherketone surface with enhanced bacteriostasis and anti-inflammatory and osseointegrative properties for implant application, Biomaterials 212 (2019) 98–114.
[30] W. Lei, K. Ren, T. Chen, X. Chen, B. Li, H. Chang, J. Ji, Polydopamine nanocoating for effective photothermal killing of bacteria and fungus upon near-infrared irradiation, Adv. Mater. Interfac. 3 (22) (2016).
[31] W.B. Tsai, C.Y. Chien, H. Thissen, J.Y. Lai, Dopamine-assisted immobilization of poly(ethylene imine) based polymers for control of cell-surface interactions, Acta Biomater. 7 (6) (2011) 2518–2525.
[32] H. Lee, S.M. Dellatore, W.M. Miller, P.B. Messersmith, Mussel-inspired surface chemistry for multifunctional coatings, Science 318 (5849) (2007) 426–430.
[33] X. Yang, M. Yang, B. Pang, M. Vara, Y. Xia, Gold nanomaterials at work in biomedicine, Chem. Rev. 115 (19) (2015) 10410–10488.
[34] Y. Cai, L. Wang, H. Hu, W. Bing, L. Tian, J. Zhao, A synergistic antibacterial platform: combining mechanical and photothermal effects based on Van-MoS(2)-Au nanocomposites, Nanotechnology 32 (8) (2021) 085102.
[35] J.T. Hsu, Y.W. Shen, C.W. Kuo, R.T. Wang, L.J. Fuh, H.L. Huang, Impacts of 3D bone-to- implant contact and implant diameter on primary stability of dental implant, J. Formos. Med. Assoc. 116 (8) (2017) 582–590.
[36] M. Li, J. Bai, H. Tao, L. Hao, W. Yin, X. Ren, A. Gao, N. Li, M. Wang, S. Fang, Y. Xu, L. Chen, H. Yang, H. Wang, G. Pan, D. Geng, Rational integration of defense and repair synergy on PEEK osteoimplants via biomimetic peptide clicking strategy, Bioact. Mater. 8 (2022) 309–324.
[37] S. Mo, K. Tang, Q. Liao, L. Xie, Y. Wu, G. Wang, Q. Ruan, A. Gao, Y. Lv, K. Cai, L. Tong, Z. Wu, P.K. Chu, H. Wang, Tuning the arrangement of lamellar nanostructures: achieving the dual function of physically killing bacteria and promoting osteogenesis, Mater. Horiz. 10 (3) (2023) 881–888.
[38] S. Mo, F. Zhao, A. Gao, Y. Wu, Q. Liao, L. Xie, H. Pan, L. Tong, P.K. Chu, H. Wang, Simultaneous application of diamond-like carbon coating and surface amination on polyether ether ketone: towards superior mechanical performance and osseointegration, Smart Materials in Medicine 2 (2021) 219–228.
[39] T.J. Webster, A.A. Patel, M.N. Rahaman, B. Sonny Bal, Anti-infective and osteointegration properties of silicon nitride, poly(ether ether ketone), and titanium implants, Acta Biomater. 8 (12) (2012) 4447–4454.
[40] I. Singh, G. Dhawan, S. Gupta, P. Kumar, Recent advances in a polydopamine-mediated antimicrobial adhesion system, Front. Microbiol. 11 (2020) 607099.
[41] J.H. Ryu, P.B. Messersmith, H. Lee, Polydopamine surface chemistry: a decade of discovery, ACS Appl. Mater. Interfaces 10 (9) (2018) 7523–7540.
[42] X. Bao, J. Zhao, J. Sun, M. Hu, X. Yang, Polydopamine nanoparticles as efficient scavengers for reactive oxygen species in periodontal disease, ACS Nano 12 (9) (2018) 8882–8892.
[43] S. Sarkari, M. Khajehmohammadi, N. Davari, D. Li, B. Yu, The effects of process parameters on polydopamine coatings employed in tissue engineering applications, Front. Bioeng. Biotechnol. 10 (2022) 1005413.
[44] X. Zhan, S. Li, Y. Cui, A. Tao, C. Wang, H. Li, L. Zhang, H. Yu, J. Jiang, C. Li, Comparison of the osteoblastic activity of low elastic modulus Ti-24Nb-4Zr-8Sn alloy and pure titanium modified by physical and chemical methods, Mater. Sci. Eng., C 113 (2020) 111018.
[45] A.A. Khalili, M.R. Ahmad, A review of cell adhesion studies for biomedical and biological applications, Int. J. Mol. Sci. 16 (8) (2015) 18149–18184.
[46] L.C. Xu, Y. Wo, M.E. Meyerhoff, C.A. Siedlecki, Inhibition of bacterial adhesion and biofilm formation by dual functional textured and nitric oxide releasing surfaces, Acta Biomater. 51 (2017) 53–65.
[47] X. Zhan, J. Yan, H. Tang, D. Xia, H. Lin, Antibacterial properties of gold nanoparticles in the modification of medical implants: a systematic review, Pharmaceutics 14 (12) (2022).
[48] Y. Cui, Y. Zhao, Y. Tian, W. Zhang, X. Lu, X. Jiang, The molecular mechanism of action of bactericidal gold nanoparticles on Escherichia coli, Biomaterials 33 (7) (2012) 2327–2333.
[49] M. Paesa, C. Remirez de Ganuza, T. Alejo, C. Yus, S. Irusta, M. Arruebo, V. Sebastian, G. Mendoza, Elucidating the mechanisms of action of antibiotic-like ionic gold and biogenic gold nanoparticles against bacteria, J. Colloid Interface Sci. 633 (2023) 786–799.
[50] P.K. Pandey, R. Maheshwari, N. Raval, P. Gondaliya, K. Kalia, R.K. Tekade, Nanogold-core multifunctional dendrimer for pulsatile chemo-, photothermal- and photodynamic- therapy of rheumatoid arthritis, J. Colloid Interface Sci. 544 (2019) 61–77.
[51] L.T. Lanh, T.T. Hoa, N.D. Cuong, D.Q. Khieu, D.T. Quang, N. Van Duy, N.D. Hoa, N. Van Hieu, Shape and size controlled synthesis of Au nanorods: H 2 S gas-sensing characterizations and antibacterial application, J. Alloys Compd. 635 (2015) 265–271.
[52] X. Bai, H. Sun, L. Jia, J. Xu, P. Zhang, D. Zhang, Y. Gu, B. Chen, L. Feng, Chondrocyte targeting gold nanoparticles protect growth plate against inflammatory damage by maintaining cartilage balance, Mater Today Bio 23 (2023) 100795.
[53] Z. Xiang, K. Wang, W. Zhang, S.W. Teh, A. Peli, P.L. Mok, A. Higuchi, S. Suresh Kumar, Gold nanoparticles inducing osteogenic differentiation of stem cells: a review, J. Cluster Sci. 29 (1) (2018) 1–7.
[54] Y. Zhang, N. Kong, Y. Zhang, W. Yang, F. Yan, Size-dependent effects of gold nanoparticles on osteogenic differentiation of human periodontal ligament progenitor cells, Theranostics 7 (5) (2017) 1214–1224.
[55] J. Lin, H. Zhang, Z. Chen, Y. Zheng, Penetration of lipid membranes by gold nanoparticles: insights into cellular uptake, cytotoxicity, and their relationship, ACS Nano 4 (9) (2010) 5421–5429.
[56] A. Rizzo, R. Paolillo, L. Guida, M. Annunziata, N. Bevilacqua, M.A. Tufano, Effect of metronidazole and modulation of cytokine production on human periodontal ligament cells, Int. Immunopharm. 10 (7) (2010) 744–750.
[57] L. Shakir, A. Javeed, M. Ashraf, A. Riaz, Metronidazole and the immune system, Die Pharmazie-An International Journal of Pharmaceutical Sciences 66 (6) (2011) 393–398.
[58] R. Weissleder, A clearer vision for in vivo imaging, Nat. Biotechnol. 19 (4) (2001) 316–317.
[59] J. Hu, Y. Ding, B. Tao, Z. Yuan, Y. Yang, K. Xu, X. Li, P. Liu, K. Cai, Surface modification of titanium substrate via combining photothermal therapy and

quorum-sensing-inhibition strategy for improving osseointegration and treating biofilm-associated bacterial infection, Bioact. Mater. 18 (2022) 228–241.
[60] X. Wang, J. Shao, M. Abd El Raouf, H. Xie, H. Huang, H. Wang, P.K. Chu, X.F. Yu, Y. Yang, A.M. AbdEl-Aal, N.H.M. Mekkawy, R.J. Miron, Y. Zhang, Near-infrared light-triggered drug delivery system based on black phosphorus for in vivo bone regeneration, Biomaterials 179 (2018) 164–174.
[61] X. Zhang, G. Cheng, X. Xing, J. Liu, Y. Cheng, T. Ye, Q. Wang, X. Xiao, Z. Li, H. Deng, Near-infrared light-triggered porous AuPd alloy nanoparticles to produce mild localized heat to accelerate bone regeneration, J. Phys. Chem. Lett. 10 (15) (2019) 4185–4191.
[62] J. Chen, Z.D. Shi, X. Ji, J. Morales, J. Zhang, N. Kaur, S. Wang, Enhanced osteogenesis of human mesenchymal stem cells by periodic heat shock in self-assembling peptide hydrogel, Tissue Eng. 19 (5–6) (2013) 716–728.
[63] K. Ikuta, H. Urakawa, E. Kozawa, S. Hamada, T. Ota, R. Kato, H. Honda, T. Kobayashi, N. Ishiguro, Y. Nishida, In vivo heat-stimulus-triggered osteogenesis, Int. J. Hyperther. 31 (1) (2015) 58–66.
[64] J. Zhang, X. Gao, D. Ma, S. He, B. Du, W. Yang, K. Xie, L. Xie, Y. Deng, Copper ferrite heterojunction coatings empower polyetheretherketone implant with multi-modal bactericidal functions and boosted osteogenicity through synergistic photo/Fenton-therapy, Chem. Eng. J. 422 (2021).
[65] L. Xie, G. Wang, Y. Wu, Q. Liao, S. Mo, X. Ren, L. Tong, W. Zhang, M. Guan, H. Pan, P.K. Chu, H. Wang, Programmed surface on poly(aryl-ether-ether-ketone) initiating immune mediation and fulfilling bone regeneration sequentially, Innovation 2 (3) (2021) 100148.
[66] Y. Zheng, A. Gao, J. Bai, Q. Liao, Y. Wu, W. Zhang, M. Guan, L. Tong, D. Geng, X. Zhao, P.K. Chu, H. Wang, A programmed surface on polyetheretherketone for sequentially dictating osteoimmunomodulation and bone regeneration to achieve ameliorative osseointegration under osteoporotic conditions, Bioact. Mater. 14 (2022) 364–376.
[67] R. Shen, R. Jia, W. Liu, Q. Lin, Y. Hai, Z. He, The function and regulation of BMP6 in various kinds of stem cells, Curr. Pharmaceut. Des. 21 (25) (2015) 3634–3643.
[68] Y. Gao, Q. Ding, W. Li, R. Gu, P. Zhang, L. Zhang, Role and mechanism of a micro-/nano-structured porous zirconia surface in regulating the biological behavior of bone marrow mesenchymal stem cells, ACS Appl. Mater. Interface 15 (11) (2023) 14019–14032.
[69] K.W. Zhang, Y. Jia, Y.Y. Li, D.Y. Guo, X.X. Li, K. Hu, X.X. Qian, Z.H. Chen, J.J. Wu, Z.D. Yuan, F.L. Yuan, LEP and LEPR are possibly a double-edged sword for wound healing, J. Cell. Physiol. 238 (2) (2023) 355–365.
[70] H.H. Pulkkinen, M. Kiema, J.P. Lappalainen, A. Toropainen, M. Beter, A. Tirronen, L. Holappa, H. Niskanen, M.U. Kaikkonen, S. Yla-Herttuala, J.P. Laakkonen, BMP6/TAZ-Hippo signaling modulates angiogenesis and endothelial cell response to VEGF, Angiogenesis 24 (1) (2021) 129–144.
[71] A. Micera, A. Lambiase, B. Stampachiacchiere, S. Bonini, S. Bonini, F. Levi-Schaffer, Nerve growth factor and tissue repair remodeling: trkA(NGFR) and p75 (NTR), two receptors one fate, Cytokine Growth Factor Rev. 18 (3–4) (2007) 245–256.
[72] Z. Alkhayal, Z. Shinwari, A. Gaafar, A. Alaiya, Fluconazole-induced protein changes in osteogenic and immune metabolic pathways of dental pulp mesenchymal stem cells of osteopetrosis patients, Int. J. Mol. Sci. 24 (18) (2023).
[73] W. Yu, C. Qian, X. Jiang, F. Zhang, W. Weng, Mechanisms of stem cell osteogenic differentiation on TiO2 nanotubes, Colloids Surf. B Biointerfaces 136 (2015) 779–785.
[74] C.C. Zhao, Q.J. Han, H.Y. Ying, X.X. Gu, N. Yang, L.Y. Li, Q.Z. Zhang, TNFSF15 facilitates differentiation and polarization of macrophages toward M1 phenotype to inhibit tumor growth, OncoImmunology 11 (1) (2022) 2032918.
[75] M. Si, J. Lang, The roles of metallothioneins in carcinogenesis, J. Hematol. Oncol. 11 (1) (2018) 107.
[76] L. Endo-Munoz, A. Cumming, S. Sommerville, I. Dickinson, N.A. Saunders, Osteosarcoma is characterised by reduced expression of markers of osteoclastogenesis and antigen presentation compared with normal bone, Br. J. Cancer 103 (1) (2010) 73–81.
[77] C.H. Shin, M.G. Lee, J. Han, S.I. Jeong, B.K. Ryu, S.G. Chi, Identification of XAF1-MT2A mutual antagonism as a molecular switch in cell-fate decisions under stressful conditions, Proc. Natl. Acad. Sci. U. S. A. 114 (22) (2017) 5683–5688.
[78] P. Li, Z. Hao, J. Wu, C. Ma, Y. Xu, J. Li, R. Lan, B. Zhu, P. Ren, D. Fan, S. Sun, Comparative proteomic analysis of polarized human THP-1 and mouse RAW264.7 macrophages, Front. Immunol. 12 (2021) 700009.
[79] Q. Liu, C. Yang, S. Wang, D. Shi, C. Wei, J. Song, X. Lin, R. Dou, J. Bai, Z. Xiang, S. Huang, K. Liu, B. Xiong, Wnt5a-induced M2 polarization of tumor-associated macrophages via IL-10 promotes colorectal cancer progression, Cell Commun. Signal. 18 (1) (2020) 51.
[80] L. Tong, Q. Liao, Y. Zhao, H. Huang, A. Gao, W. Zhang, X. Gao, W. Wei, M. Guan, P. K. Chu, H. Wang, Near-infrared light control of bone regeneration with biodegradable photothermal osteoimplant, Biomaterials 193 (2019) 1–11.
[81] J. Peng, J. Zhao, Q. Tang, J. Wang, W. Song, X. Lu, X. Huang, G. Chen, W. Zheng, L. Zhang, Y. Han, C. Yan, Q. Wan, L. Chen, Low intensity near-infrared light promotes bone regeneration via circadian clock protein cryptochrome 1, Int. J. Oral Sci. 14 (1) (2022) 53.